



universität
wien

MASTERARBEIT

Titel der Masterarbeit

Synthesis and optical properties of SWCNTs doped by Boron and Nitrogen Heteroatoms

angestrebter akademischer Grad

Master of Science (MSc)

Verfasserin / Verfasser: Rosa Georgina Ruiz Soria
Matrikel-Nummer: 0963022
Studienrichtung (lt. Studienblatt): Physics
Betreuer: Prof. Thomas Pichler

Wien, im Juli 2010

To my mother and my sister

Table of Contents

Table of Contents	v
Acknowledgements	vii
Zusammenfassung	viii
Abstract	ix
Introduction	1
1 General Aspects	2
1.1 Carbon	2
1.2 Single-walled carbon nanotubes	3
1.2.1 Electronic Structure of SWCNTs	3
1.2.2 Electronic properties	6
1.3 Modification of the electronic properties of SWCNTs	8
1.3.1 Intercalation	8
1.3.2 Endohedral Functionalization	8
1.3.3 On-wall doping	9
2 Methods	11
2.1 Synthesis	12
2.1.1 A word on growth mechanisms	12
2.1.2 Synthesis methods	12
2.1.3 Post growth doping via N_2^+ Ion implantation	14
2.2 N-Doped SWCNTs studied in this thesis	15
2.2.1 AA-CVD: <i>Ferrocene Reactor</i>	16

2.2.2	Boron doped SWCNTs synthesized via high vacuum chemical vapor deposition	18
2.3	Characterization tools	19
2.3.1	SEM, TEM and TEM-EELS	19
2.3.2	X-ray photoelectron spectroscopy (XPS)	21
2.4	Optical Techniques	21
2.4.1	Raman Spectroscopy	22
2.4.2	Optical absorption	26
2.4.3	Photoluminescence	27
2.4.4	Equipment used in the thesis	28
3	Results and Discussion	31
3.1	N doped nanotubes	31
3.1.1	Overall Morphology	31
3.1.2	Analysis of mean diameter and diameter distribution of doped nanotubes	33
3.1.3	N content and bonding environment on samples	37
3.2	B doped nanotubes	40
3.2.1	Overall Morphology	40
3.2.2	Optical properties, defects concentration and doping level from Raman	42
4	Conclusions & Future Perspectives	45
	Bibliography	46

Acknowledgements

I thank all the people who supported me during the time I have needed to carry on this work. First of all, I am grateful to Prof. Thomas Pichler for giving me the opportunity to do this work at his group. This opportunity allowed me to travel abroad and meet and interact with scientists from all around the world, which was crucial and important in the process of my training as a physicist. The good training that I received here -both intellectually and personally- , helped me to develop my skills and knowledge needed in a world where the "state of the art technology" is greatly appreciated. Additionally, my master studies in Austria were done within the group Elektronische Materialeigenschaften from the Fakultät für Physik at the University of Vienna, under the financial support of the project DFG PI 440/5. I would like to give a special thanks to my immediate supervisor and good friend, Dr. Paola Ayala, for first arousing my interest in the world of nanotubes and then spending endless amounts of time working hard side by side to carry out this work successfully. She showed me that researching is a game where we are allowed to imagine and to be creative. She could see all my dreams and expectations, so she always tried to nurture them and help me to become them truth by my own effort...she gave my wings and taught me to fly. Furthermore, I would like to thank all my colleagues, and now friends, at the group: Dr. Xianje Liu, Dr. Feri Simon, Dr. Christian Kramberger, Joonas Parjane, from whom I have learnt part of the art of nanoscience. I also greatly appreciate the assistance from the technical staff of the group. Of course, I would like to thank my mother, Rosa and my sister, Rosita for their support throughout my life and for all their love and patience. They are the only motivation I need to go through life fighting for my dreams. I am grateful to all my family because they were always by my side when I needed. Finally, I wish to thank all those friends- from Argentina and all around the world- who spent many nights giving me strength to go on.

Vienna, Austria
July, 2010

Georgina Ruiz Soria

Zusammenfassung

Diese Masterarbeit beschäftigt sich hauptsächlich mit der Studie von single walled-carbon nanotubes (SWCNTs) sowie mit der Änderung deren elektronischer Eigenschaften, hervorgerufen durch deren Dotierung mit N beziehungsweise B. Hinsichtlich der Synthese von Nanoröhren existiert bereits eine breite Menge an Literatur, welche sich in erster Linie mit multi-walled nanotubes-Strukturen beschäftigt. Obwohl die meisten jener Studien auch von der Verwendung von single-walled nanotubes sprechen, haben die experimentellen Methoden um solche Strukturen zu erhalten erst kürzlich die bisherigen Schwierigkeiten bei der Synthese von dotierten single-walled carbon nanotubes überwunden. Aus diesem Grund wird die umfassende Charakterisierung gerade dieser relativ neuen Materialien dringend benötigt.

In der vorliegenden Arbeit wurden unterschiedliche Arten von SWCNTs, welche mittels diverser spektroskopischer Techniken mit Stickstoff dotiert wurden, untersucht. *In situ* wurde die Dotierung während des Wachstums in N-dotierten SWCNTs studiert, wobei in diesem Fall hauptsächlich die chemical vapor deposition auf zwei verschiedene Arten als Synthesemethode angewendet wurde. Des Weiteren wurde die SWCNTs-Dotierung mit N auch nach deren Synthese an einem pristine laser ablation SWCNTs buckypaper untersucht, wobei N_2^+ Ionen implantiert wurden. Im Zuge dieses Projektes wurde ebenso versucht die kontrollierte Synthese B-dotierter single-walled nanotubes mittels der high vacuum chemical vapor deposition-Methode zu optimieren. Die optischen und elektronischen Eigenschaften dieser Nanoröhren wurden einerseits durch spektroskopische Techniken (optische Absorption, Multi-Frequenz Raman-spektroskopie, Photoluminiszenz) als auch mittels zusätzlicher, dazu komplementärer Studien, durchgeführt im Zuge der Zusammenarbeit mit diversen anderen Gruppen (XPS, TEM, EELS), auf welche in späteren Textpassagen noch weiter eingegangen wird, analysiert.

Abstract

This master thesis is mainly focused on the study of single walled-carbon nanotubes (SWCNTs) and the changes of their electronic properties upon doping with N and B. The literature related to the topic of synthesis is relatively vast regarding multi-walled nanotube structures. However, although most of the theoretical studies involve the use of single walled material, the experimental methods to obtain such structures have only recently overcome the difficulties to synthesize doped single-walled carbon nanotubes. For this reason, an extensive characterization of these relatively new materials is still urgently required.

In this work, different kinds of SWCNTs doped with nitrogen via different spectroscopic techniques have been studied. *In situ* doping during growth was studied in N-doped SWCNTs, in which case the main synthesis method was chemical vapor deposition in two different types. Additionally, post synthesis doping with N on SWCNTs was studied on a buckypaper of pristine laser ablation SWCNTs where N_2^+ ion implantation was applied. During this project, the controlled synthesis of single-walled nanotubes doped with B was optimized via the high vacuum chemical vapor deposition method. The optical and electronic properties of these nanotubes were examined also by the spectroscopic techniques (optical absorption, multi-frequency Raman spectroscopy, photoluminescence), and complemented with additional studies done via collaborations (XPS, TEM, EELS), which will be mentioned along the text where it applies.

Introduction

Carbon nanotubes take undoubtedly a leading position in the nanotechnology research due to their well known outstanding structural and electronic properties. Inspired on this, hybrid and functionalized tubular structures have been thought via several modification paths that involve the presence of molecules, generation of defects and partial or full replacement of the carbon atoms but always maintaining a nanotube structure. The possibilities are countless but in this case it has been mainly dealt with the case of functionalization by substitutional doping with Boron and Nitrogen.

N contains one additional electron compared to C. The same way of thinking applies to B, which lacks one electron, thus novel electronic properties can be expected if N and B atoms directly substitute C atoms in the graphitic lattice of SWCNTs. Depending on the amount of atoms incorporated it is possible to think about low or high doping regimes. The samples, studied in this work, contain a very low dopant concentration. The effects of dopant amounts are described in the first chapter of this thesis. For now, it is more important to briefly remark on the experimental difficulties to obtain doped SWCNTs.

In all semiconductor applications, the properties of a device depend on the control of the electronic states in the valence and conduction bands for design and optimization purposes. Doping with heteroatoms is a well established technique in Si technology to achieve this objectives. It is well known that doping with electron donors or acceptors leads to a very sensitive shift of the Fermi level considering the presence of heteroatoms in parts per million. If the electronic properties of SWCNT depend strongly, as expected, on the substitution of heteroatoms, then the controlled synthesis of p- and n-type material should be feasible with analogue methods. In this context, the outstanding physical properties of pristine SWCNT have been very well studied [1, 2, 3, 4, 5, 6], but if these novel structures are to fulfill their promise in real applications within the semiconductor industry then it is mandatory to be able to control their electronic properties. One of the proposed methods is the insertion of dopants such as N and B as in our case of study [7, 8, 9].

Chapter 1

General Aspects

1.1 Carbon

Apart from being the most abundant element in nature, carbon is the sixth element of the periodic table and the one with the lowest atomic number of any element in the column IV. Its electronic configuration is $1s^2 2s^2 2p^2$, which allows it to form structures with various geometrical arrangements. Carbon atoms play the role of "lego pieces", which can be put together to form different structural arrangements such as graphite, diamond, fullerenes or nanotubes. More related to this work, CNTs are molecular nanostructures that are unique for several of their physical properties.

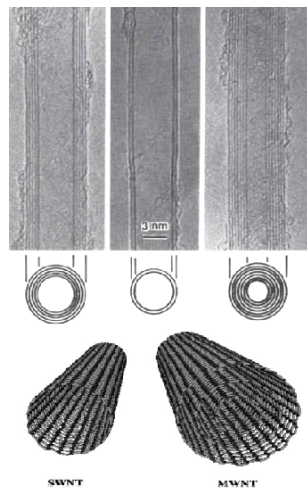


Figure 1.1: The TEM images correspond to the micrographs that Iijima first reported in 1991 [4]. These pictures correspond to multi-walled nanotubes with different inner and outer diameters and number of cylindrical shells. The lower molecular models correspond to a single- and a multi-walled CNT.

1.2 Single-walled carbon nanotubes

As already mentioned, both SW- and MWCNTs are one-dimensional (1D) structures with defined electronic, molecular and structural properties, in turn very different in each of the particular species (see molecular models in Figure 1.1). The literature related to carbon nanotubes is countless so the following sections are simply aimed at summarizing the electronic structure of SWCNTs, their physical properties and mostly their controlled modification. This section briefly describes the properties of SWCNTs based on the graphene structure as parent material. Attention is given to the changes on the SWCNT electronic properties upon specific on wall doping.

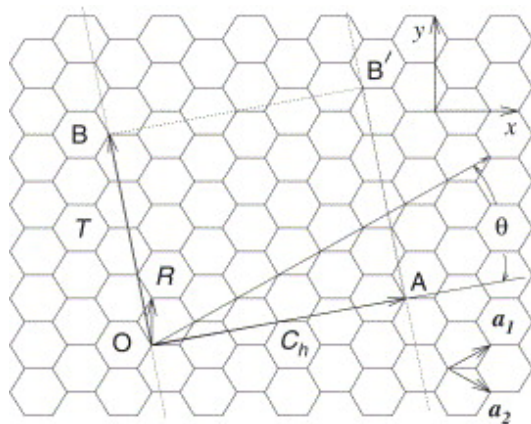


Figure 1.2: Honeycomb lattice. The vectors OA define the chiral angle C_h and the OB , the translational vector T . The chiral angle θ is the angle between the chiral vector and the the zigzag direction of the graphene lattice [10].

1.2.1 Electronic Structure of SWCNTs

It is reasonable to start focusing on the structure of graphene, which is a 2D layered arrangement of atoms distributed in a hexagonal lattice [10], usually known as the "honeycomb lattice", which is depicted in (Figure1.2). This planar configuration is mainly given by the sp^2 type of hybridization existing in C atoms. This is extremely important in these structures, since the type of bond between these hybrid orbitals of the carbon atoms is what forms the backbone structure of SWCNTs.

A SWCNT can be imagined as a rolled-up graphene sheet [10]. So, taking as reference the honeycomb lattice, the structure of a SWCNT can be determined by the so called chiral vector \vec{C}_h (Figure 1.2). This vector $\vec{C}_h = n\vec{a}_1 + m\vec{a}_2$ defines the circumference of the nanotube connecting two crystallographically equivalent sides on the graphene sheet. It depends on its pair of indices (n,m) , which denote the number of unit vectors along two directions in the honeycomb crystal lattice of graphene. This chiral can be expressed in \vec{a}_1 and \vec{a}_2 , which are the unit vectors of the hexagonal

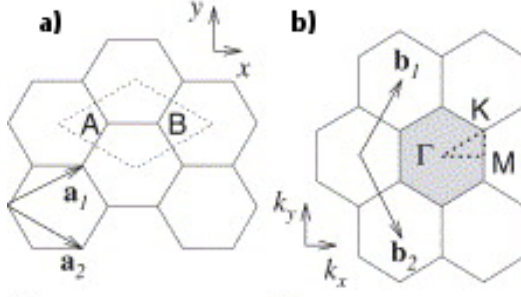


Figure 1.3: **a)**Real lattice of a SWCNTs. The dotted rhombus shows where carbons are located in the unit cell (sites **A** and **B**). **b)**reciprocal lattice. The shaded hexagon represent the Brillouin zone of the graphene sheet. The high symmetry points (Γ , **K** and **M**). a_i and b_i ($i = 1, 2$) are basis and reciprocal lattice vectors [11]

lattice depicted in figure 1.3. Additionally, the diameter d_h of the nanotube is given by the following equation:

$$d_h = \frac{|C_h|}{\pi} = \frac{\sqrt{3}a_{C-C}}{\pi} \sqrt{n^2 + nm + m^2} \quad (1.2.1)$$

where a_{C-C} is the bond length ($a_{C-C} = 1,42\text{\AA}$).

The chiral angle θ (the angle between \vec{C}_h and \vec{a}_1) is always taken starting from the zigzag direction. This angle can be calculated from:

$$\cos\theta = \frac{\vec{C}_h \cdot \vec{a}_1}{|\vec{C}_h| |\vec{a}_1|} = \frac{2n + m}{2\sqrt{n^2 + nm + m^2}} \quad (1.2.2)$$

This chiral vector denotes the tilt angle of the hexagons with respect to the direction of the nanotube axis (Figure 1.2). It is possible to classify the nanotubes taking into account the chiral angle[12].

At $\theta = 0^\circ$, they are called *zigzag nanotubes* given by the zigzag pattern they exhibit along the circumference. Then, at $\theta = 30^\circ$, they are of the type (n, n) and they are called *armchair nanotubes*. In this case, they show an armchair pattern along the circumference. For all others angles between $0^\circ < \theta < 30^\circ$, they are called *chiral nanotubes*.

The geometry of the graphene lattice and the chiral angle also determine the unit cell and its number of carbon atoms. The smallest graphene lattice vector \vec{T} perpendicular to \vec{C}_h defines the translational period t along the tube axis.

The lattice vector \vec{T} can be expressed in terms of the basis vectors \vec{a}_1 and \vec{a}_2 as $\vec{T} = t_1 \cdot \vec{a}_1 + t_2 \cdot \vec{a}_2$, where t_1 and t_2 are integers. Using $\vec{C}_h \cdot \vec{T} = 0$, this integers can be expressed as a function of the indices n and m as

$$t_1 = \frac{2m + n}{N_R}, t_2 = \frac{2n + m}{N_R} \quad (1.2.3)$$

where N_R is the greatest common divisor of $(2m + n)$ and $(2n + m)$.

Considering the unit cell as a rolled-up rectangle spanned by \vec{C}_h and \vec{T} , the number of electronic and phononic bands in SWCNTs can be denoted by obtaining the number of hexagons per unit cell N_C . This number can be expressed as a function of n and m and since every hexagon contains two carbon atoms, its value results as

$$N_C = \frac{4(n^2 + nm + m^2)}{N_R} \quad (1.2.4)$$

The lattice vector \vec{T} and the chiral vector \vec{C}_h determine the unit cell of the carbon nanotube in real space and the corresponding vectors in reciprocal space are the reciprocal lattice vectors \vec{K}_2 along the nanotube axis and \vec{K}_1 in the circumferential direction. These vectors can be obtained from the relation $\vec{R}_i \cdot \vec{K}_j = 2\pi\delta_{ij}$, where \vec{R}_i and \vec{K}_j are the lattice vectors in real and reciprocal space, respectively.

So, the Brillouin zone of SWCNTs is calculated from these resulting relations:

$$\vec{C}_h \cdot \vec{K}_1 = 2\pi, \vec{T} \cdot \vec{K}_1 = 0, \vec{C}_h \cdot \vec{K}_2 = 0, \vec{T} \cdot \vec{K}_2 = 2\pi \quad (1.2.5)$$

The resulting Brillouin zone is then a system of parallel lines with a length of $|\vec{K}_2|$ and a spacing of $|\vec{K}_1|$. The length of the parallel lines is given by $\frac{2\pi}{|\vec{T}|}$.

The reciprocal lattice vectors can be expressed as a function of \vec{b}_1 and \vec{b}_2 , which are the reciprocal lattice vectors of a 2D graphene sheet. Two wave vectors which differ by $N\vec{K}_1 = (-t_2\vec{b}_1 + t_1\vec{b}_2)$ are equivalent because this vector corresponds to a reciprocal lattice vector of 2D graphite. The $N - 1$ wave vectors which differ by $\mu\vec{K}_1$ with $\mu = 1, 2, \dots, N - 1$ are not equivalent as t_1 and t_2 do not have a common divisor except unity. The reciprocal lattice vector can thus be expressed as

$$\vec{K} = k \frac{\vec{K}_2}{|\vec{K}_2|} + \mu \vec{K}_1, -\frac{\pi}{|\vec{T}|} < k < \frac{\pi}{|\vec{T}|} \quad (1.2.6)$$

As a result of the periodic boundary conditions along the circumference, N discrete k vectors perpendicular to the nanotube axis are obtained. Continuous wave vectors are allowed along the axis provided an infinite length of the nanotube is assumed.

1.2.2 Electronic properties

As thoroughly described in the previous section, the electronic structure of a nanotube can be obtained from the one of 2D graphite, but the quantum confinement of the 1D electronic states has to be taken into account. Due to the existence of discrete wave vectors, the SWCNT energy bands consists of N 1D energy dispersion relations which fulfill the condition for the allowed states for \vec{K} . These lines are cross sections of those for 2D graphene and are obtained by simply replacing the wave vector k in the graphite energy dispersion with the allowed wave vectors. This method is called *zone – folding* (see Fig 1.4).

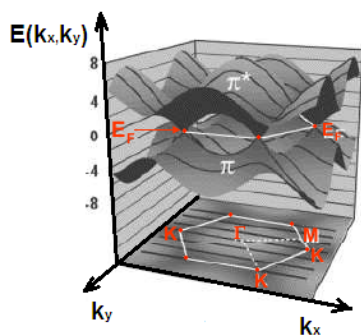


Figure 1.4: The zone-folding scheme. Here, it is shown the energy dispersion along the high symmetry lines. The π and π^* bands are degenerate at the K points (Fermi energy) in the hexagonal Brillouin zone. [10].

At the bottom of the figure, the first Brillouin zone of the graphene sheet with the allowed states for an (3, 3) armchair nanotube (thick line) is represented. A rectangle is formed in the Brillouin zone and is associated with the four-atom cell. In a simplified manner, to obtain the (3, 3) band structure in the band-folding approach, it is necessary to fold the corner of the zone onto the rectangular cell and superimpose the graphene energy bands calculated along the obtained thick lines. Above, it is represented the dispersion relations $E^\pm(k_x, k_y)$ for the graphene plane, together with that of an armchair nanotube (thick line). Here, the Fermi surface is reduced to the six distinct \mathbf{K} points of the hexagonal Brillouin zone and the bonding π (last valence) band and the antibonding π^* (first conduction) band cross at the vertices of this zone.

The position and direction of the allowed SWCNT k states with respect to the graphene Brillouin zone depend on the direction in which the nanotube is rolled up. So it can be predicted that different SWCNT chiralities have different electronic band structures, if the cutting lines cross the K-point of the graphene Brillouin zone. This is inferrable because the K- point is the only point where the graphite π band crosses the Fermi level. So if a cutting line crosses the K-point, the resulting SWCNT is metallic because its band structure also contains a band which crosses the Fermi level. If the line does not cross the K-point, the SWCNT is semiconductor since a gap appears in its band structure.

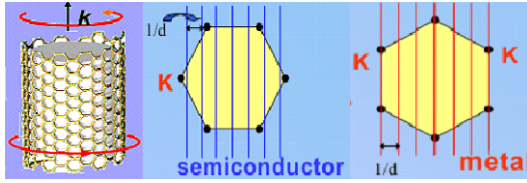


Figure 1.5: SWCNTs are classified as metallic or semiconducting nanotubes, since the cutting lines crosses (or not) the K point.

SWCNTs can be grouped in *classes* (Figure1.5), according to this simple rule $\text{mod}(2n+m, 3) = 0, 1, 2$, where 0,1,2 are integers denote the remainders when $(2n+m)$ (representing the SWCNT *families*) is divided by 3.

If $\text{mod}3 = 0$, they are metallic (allowed \vec{k} vector crosses the K point) and if $\text{mod}3 = 1$ or $\text{mod}3 = 2$, they are two types of semiconductors (no allowed k vector crosses the K point). All the armchair nanotubes are metallic.

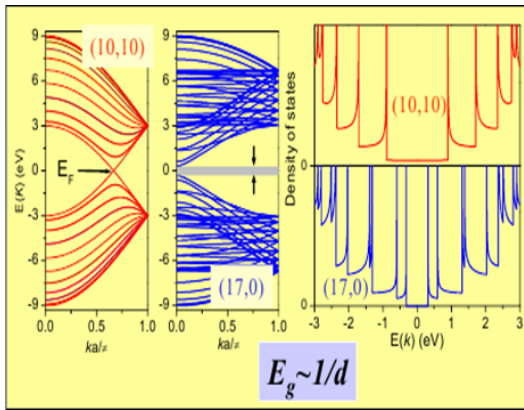


Figure 1.6: Band structure and density of states for a (10,10) armchair and a (17,0) zigzag nanotube within the zone folding model.

In the electronic density of states (DOS), the most prominent features are the spikes called *van Hove singularities* (vHs)(Figure 1.6)[10, 1]. The vHs are of great importance for the spectroscopic investigation and characterization of SWCNTs since they favor the analysis of the optical experiments. The vHs closer to the Fermi level originate from the cutting lines closer to the K point in the 2D Brillouin zone. So their most important property is that the gap between corresponding vHs scales with the inverse diameter. The allowed k -vectors in a SWCNT are the cutting lines of the graphite band structure. If a SWCNT is large enough, these cutting lines are close enough to assume that the dispersion of graphite is linear between them. The cutting lines, and consequently the positions where the bands are flat and lead to vHs in the DOS , are thus equidistant in energy. The transition energies between corresponding vHs are then given by

$$E_{ii} = \frac{2ia_0\gamma_0}{d} \quad (1.2.7)$$

where i is a multiple of three belong to metallic tubes, the others to the semiconducting tubes.

If the E_{ii} values for all the (n, m) SWCNTs or their diameter, calculated by the tight binding model, are known, the Kataura plot [13] can be used to interpret the optical spectra from carbon nanotubes.

1.3 Modification of the electronic properties of SWCNTs

The properties of single-walled nanotubes can be modified in a variety of ways. In the case of the modification of the electronic properties, various functionalization paths can be thought and one of this is doping with electron acceptors or donors [9] envisaging the use in semiconductor technology. In the next paragraphs a description of few different functionalization methods will be done and the one used in this thesis will be explain in more detail.

1.3.1 Intercalation

In the case of intercalation, a SWCNTs bundle allow the presence of atoms and small molecules in its interstitial channels. The bundle properties is modified by this way of doping, since the guest atoms (or molecules) can be electron-donors or electron-acceptors.

1.3.2 Endohedral Functionalization

This functionalization method involves the encapsulation of atoms, molecules or crystalline materials inside nanotube hollow core. (See Figure 1.7), which shows one of the classical examples of material encapsulated in a SWCNT. These are the so called peapods, which consist of fullerenes encaged in the hollow core of the SWCNTs. The electronic structures of the peapods as such differs drastically from that of pristin SWCNTs, and they can be seen as endohedrally doped from that point of view. Another example is the complete filling of the hollow core. Ajayan and Iijima [14] reported the filling of MWNT cores which by heating the tubes in air together with metallic lead. The filling of carbon nanotubes has been a very active field and has been reviewed elsewhere. Furthermore the encapsulation of organic molecules inside SWNTs is tested intensively. Hybrid systems have been reported with modified electronic and optical properties, although there are still some difficulties preparing

homogeneous samples.

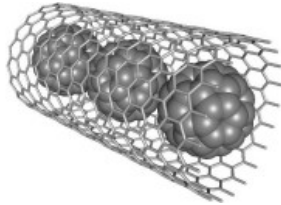


Figure 1.7: The peapod is an example of a endohedrally functionalized nanotube. The hollow core of the SWCNT is filled in this case with fullerenes [15].

1.3.3 On-wall doping

The crystalline wall of the SWCNT can be modified incorporating different atoms, or even inducing deformation of the pure C network leading to a rearrangement of the structure of the hexagons of the honeycomb lattice. In this case, where the dopant is a heteroatom which takes the place of one the C atoms in the lattice, the functionalization path is called "substitutional functionalization". An illustration of this is depicted in figure 1.8. The properties changes will show strong dependence on the site and the amount of dopant incorporated.

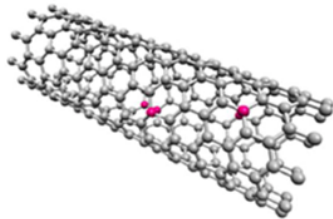


Figure 1.8: This figure shows the incorporation of an foreign atoms in the wall of the CNT [15].

Substitutional doping: Doping CNTs with B and N

This work focuses mainly on analyzing the effects of boron and nitrogen on wall substitution of carbon atoms on the SWCNT wall. Therefore, the case of N- and B-doping as a subset of the on-wall functionalization methods has been dealed. However, this does not exclude further possibilities arising due to the presence of B and N atoms, such as the formation of heteronanotubes, but they are not discussed here. Due to their similarity in size with C atoms, B and N atoms have been always considered as natural dopants [16, 17]. Nitrogen has one more electron in comparison to carbon, therefore it would be expected that direct substitution of N atoms leads n-type doping.

This means that this substitution leads to the generation of localized energy states above the Fermi level (donor state). Nevertheless, a different case can be considered which is the on-wall formation of the so called pyridinic sites. In this case, three coordinated N atoms form a localized defect which has been predicted to lead to p-type doping depending on the amount and distribution of the dopant sites.

On the other hand, a SWCNT can be doped by replacing a C atoms with B ones. Although domains of B can be formed along the structure causing another kind of changes in the electronic structure [18, 19]. The direct substitution of low concentration of B produces the formation of energy states below the Fermi level (acceptor states) very near the valence band edge[20, 21].

Low doping and the Rigid Band Model

The amount of dopant plays a very important role in the modification of the electronic structure of CNTs. Low and high doping produce critical differences in the physical properties of the nanotubes. In order to apply SWCNTs as substitutes in semiconductor technology, it would be ideal to control their semiconducting properties still considering the principles of a rigid band model such as in Si technology. With this, it is possible to simply consider a shift of the Fermi level in the band structure of the pristine system towards the valence or the conduction bands.

High doping and formation of heteronanotubes

The aim of this thesis is the study of the doping effects focusing on the low doping level case. However, in the case in which the incorporation of heteroatom is higher, two situations are possible: High doping and formation of novel heteronanotubes.

A heteronanotube of B, C and N is a 1D tubular structure with an essentially similar overall morphology compared to SWCNTs and the basic picture of a tubule with the honeycomb-like wall structure [22, 23]. However this wall structure is in principle a stable planar layer of C, B and N atoms arranged in hexagonal distribution with various stoichiometries. With the aid of an example, it will be easier to understand the concept of high doping and heteronanotubes. BC_3 -SWCNT is not a highly B doped nanotube. In this case, due to the high doping, a BC_3 planar graphite-like stable sheet is formed. Other examples of heteronanotubes theoretically predicted, are BC_2N , C_3N_4 , among others.

Chapter 2

Methods

The importance and impact of the discovery of SWCNTs is definitely a great motivation to research how to make it possible to manipulate their properties of CNTs and improve them. Carbon nanotubes attract much interest for their potential applications deriving from their unusual structural and electronic properties. As already mentioned these properties are directly related to the atomic structure of the tube. Therefore, when producing nanotube material, it is important to understand what controls the nanotube morphology (diameter, helicity and structure) during the synthesis. In this work are reported on the modifications due to the incorporation of B and N using different synthesis methods[9, 24, 25, 7]. Different synthesis methods were used to produce the samples studied here. N-doped nanotube samples obtained with two different variations of aerosol assisted chemical vapor deposition (CVD) were used (these samples were provided by the NMG group at Aalto university in Finland). Additionally, mats of pristine laser ablation SWCNTs doped via ion implantation were provided by collaboration with PUC-Rio (Brazil) and IFW-Dresden (Germany). Finally, B doped samples produced in house with high vacuum -CVD, were optimized and characterized.

With each method, it is expected that the morphology regarding bundle formation and diameter distribution is different. Additionally, the dopant concentration and dopant distribution in each case determine the electronic behavior of the bundles and the individual nanotubes.

2.1 Synthesis

The synthesis of pristine carbon nanotubes is the subject of several years of research. Great advances have been observed in the last two decades and nowadays pristine material can be synthesized, purified and even sorted regarding metallicity. The complexity of introducing dopants in a controllable manner makes the synthesis of doped nanotubes still a challenge to overcome. In this section is briefly reviewed the synthesis for pristine nanotubes and later deepen into the methods here utilized for the production of doped material. Although it is crucial to understand the formation mechanisms of the CNTs to design procedures which allow controlling the growth conditions, this work mainly focuses on obtaining material that allows us to study the physical properties rather than optimizing a mass production.

2.1.1 A word on growth mechanisms

The way in which nanotubes are formed is not exactly known. The grown is still a subject of controversy, and more than one mechanism might be operative during the formation of CNTs. The exact atmospheric conditions and the catalysts used depends on the technique, and determine if SWCNTs or MWCNTs are grown. Although a rich literature is available for the case of pristine carbon NTs, again, the information regarding doped structures is still scarce. The first hints for growth mechanisms of doped structures have started to be developed in the past two or three years.

2.1.2 Synthesis methods

As already mentioned, the synthesis methods used for the growth of pristine carbon nanotubes have been developed in various fashionable variations of the traditional techniques. The different synthesis methods and other parameters have a great influence in their properties.

The common ways to produce carbon nanotubes and these have been applied to a certain extent to the direct synthesis of CNT material doped with nitrogen and boron. This can be seen as *in situ* doping. Furthermore, it is possible to use pristine SWCNTs and use them as starting material to attempt *post growth* doping. In this case, ion implantation has been chosen to study such type of experiments. The following lines describe briefly the synthesis methods which specifically apply to the samples studied in this thesis.

Laser ablation

In this method, a graphite target is vaporized by a powerful laser in a furnace at high temperatures [26, 27]. The oven is filled with He or Ar gas in order to keep the pressure at 500 Torr. In one possible growth mechanism, a very hot plume forms, then expands and cools to form the larger clusters. The catalysts also begin to condense but more slowly at first, and attach to carbon clusters and prevent their closing into cage structures. Catalysts may even open structures when they attach to them. From this initial clusters, tubular molecules grow into SWCNTs until the catalyst particle become too large, or until conditions have cooled sufficiently that C no longer can diffuse through or over the surface of the catalyst particles. It is also possible that the particles become that much coated with C layer that they cannot absorb more and the nanotube stop growing. In this case, the SWCNT formed are bundled together by van der Waals forces. The SWCNTs produced by this method are typically with a mean diameter between 1.0 and 1.6nm, which makes them ideal for several fundamental studies and applications.

Arc discharge

This method was not used in the thesis but it is explained due to its important. It creates CNTs through arc-vaporization of two carbon rods placed end to end, separated by approximately 1 mm, in a enclosure that is usually filled with an inert gas, like He or Ar, at low pressure. A direct current creates a high temperature discharge between the two electrodes [4]. The discharge vaporizes one of the carbon rods and forms a small rod shaped deposit on the other rod. The single-layer tubules nucleate and grow on metal particles in different sizes depending on the quenching rate in the plasma. In other words, temperature and carbon and metal catalysts densities affect the diameter distribution of CNTs. The laser ablation method and arc discharge are similar due to the temperature range they involve for synthesis. The reaction conditions and the growth-mechanism are apparently very similar. However, laser vaporization results in a higher yield for SWCNTs synthesis and they appear to be more crystalline and with a narrower diameter distribution than the SWCNTs produced by the arc discharge method. With laser ablation method, cleaner nanotubes are obtained.

Chemical vapor deposition (CVD)

This method relies on the decomposition of a gaseous hydrocarbon carbon source using heat or plasma and, in the case of SWCNTs, with the aid of (molten) catalyst particles. The catalyst particles absorb the carbon, eventually leading to an over

saturation of carbon in the particle. This leads to the formation of carbon structures at the surface of the particle which tend to grow into tubes. In the perfect case, one nanotube grows from one catalyst particle. This allows spatial positioning of a nanotube by arranging the catalyst particles in a controlled way. The method can easily be up scaled for production of larger amounts of nanotube materials.

	Laser Ablation	Arc Discharge	CVD
Typical yield	up to 70%	30 to 90%	20 to 100%
Characteristics	Long bundles of tubes with individual diameters of 1-2nm	Short tubes with diameters of 0,6-1,4 nm	Long tubes with diameters of 0,6-4 nm
Advantages	Diameter control and few defects. Quite pure product	Few structural defects	Long Tubes with controllable diameters. Quite high purity. Easiest to scale up for industrial production
Disadvantages	Costly	Short tube length with random size. Significant purification is needed	

2.1.3 Post growth doping via N_2^+ Ion implantation

Ion implantation [28] is a materials engineering process by which ions of a material can be implanted into another solid, thereby changing the physical properties of the solid. It is used in semiconductor device fabrication and in metal finishing, as well as various applications in materials science research. The ions introduce both a chemical change in the target or induce a nuclear transmutation, and a structural change. A typical ion implantation equipment consists of an ion source, where ions of the desired element are produced, an accelerator, where the ions are electrostatically accelerated

to a high energy, and a target chamber, where the ions impinge on a target, which is the material to be implanted. Each ion is typically a single atom or molecule, and thus the actual amount of material implanted in the target is the integral over time of the ion current, which is the implantation dose.

The energy of the ions, as well as the ion species and the composition of the target determine the depth of penetration of the ions in the solid: A monoenergetic ion beam will generally have a broad depth distribution. The average penetration depth is called the range of the ions. Under typical circumstances ion ranges will be between 10 nanometers and 1 micrometer. Thus, ion implantation is especially useful in cases where the chemical or structural change is desired to be near the surface of the target. Based on these very important concepts, the possibility of N_2^+ implantation has been envisaged and calculated theoretically in order to produce N-doped nanotube material. The literature corresponding on theoretical studies about ion implantation as a doping method is scarce but a few papers have indeed been published, whereas regarding experimental reports, only one paper from Xu and co-workers has shown some first doping attempts on SWCNTs [28]. It has been done similar studies using an XPS analysis chamber allowing us to work in UHV. In fact, the introduction of dopants in a semiconductor is the most common application of ion implantation [29, 30]. Dopant ions such as boron, phosphorus or arsenic are generally created from a gas source, so that the purity of the source can be very high. When implanted in a semiconductor, each dopant atom can create a charge carrier in the semiconductor after annealing. A hole can be created for a p-type dopant, and an electron for an n-type dopant.

2.2 N-Doped SWCNTs studied in this thesis

In the thesis project are been carried out spectroscopic characterization of SWCNTs doped with B and N, which have been synthesized by different methods. B-doped nanotubes with a very narrow diameter distributions were synthesized in-house. In addition, materials provided through two collaborations were used:

Aerosol assisted (AA)-CVD nitrogen doped nanotubes from the Nanomaterials Group (NMG) at Aalto University in Finland. These samples have been produced with two different variations of the system.

Laser ablation pristine SWCNTs produced at the IFW-Dresden, which have later undergone ion bombardment with N_2^+ ions in a UHV analysis chamber at the van de Graaff Laboratory at PUC-Rio.

These types of materials have been compared to analyze the effects of the in situ doping with N during growth, and post doping via ion implantation. The experimental details are briefly described here below.

2.2.1 AA-CVD: *Ferrocene Reactor*

As a variant of a conventional CVD [31, 32, 33, 34], AA-CVD involves atomization of a liquid precursor into fine aerosol droplets that are delivered to a heated zone where evaporation, decomposition and subsequent CVD reactions occur, leading to the deposition of a stable solid product. In AA-CVD, chemical precursors do not necessarily need to be volatile, but merely soluble in any solvent from which the aerosol can be generated. The synthesis of the N-doped SWCNTs, was performed in a vertical laminar flow reactor (Figure 2.1). The experimental set-up uses the catalyst

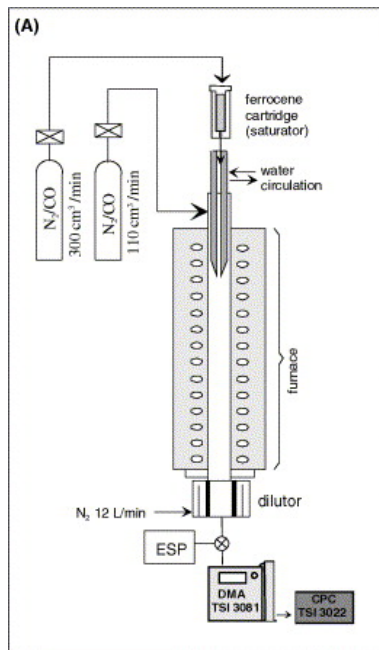


Figure 2.1: Vertical laminar flow reactor from TKK. N-doped SWCNTs produced via AA-CVD using this experimental set-up were studied in this thesis. [35]

particle formation via thermal decomposition of ferrocene consisting of a saturator, a water-cooled injector probe, and a furnace. The details for this setup can be found in [35] and the synthesis parameters to produce the nanotubes here studied have been reported in reference by T. Susi et al.

Hot Wire Generator (HWG)

The basic idea of the method is to produce catalyst particles by a physical vapour evaporation-nucleation-condensation technique and to introduce the pre-made particles into the conditions favorable for the CNT formation. For the synthesis of catalyst

particles the hot wire particle generator with iron or nickel wire can be used. Carbon monoxide, natural gas or alcohols can be used as a carbon source.

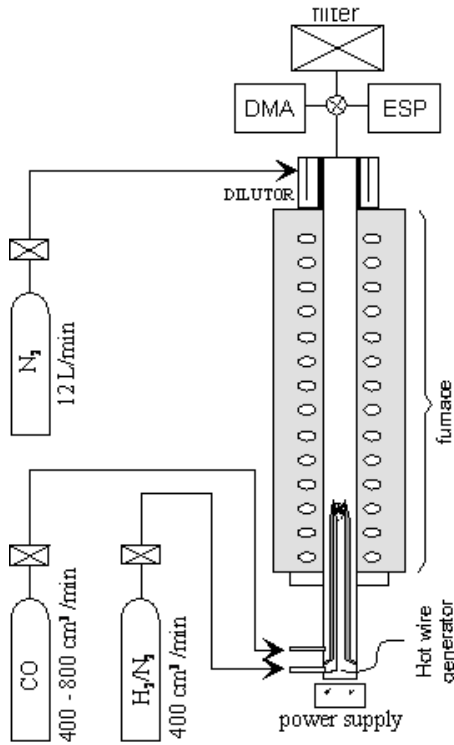


Figure 2.2: Hot Wire Generator (HWG) set up (from Aalto University in Finland). This image was adapted from [35].

The embodiment of the experimental setup consists of a HWG and a heated vertical tubular reactor (Figure 2.2). A ceramic tube inserted inside a furnace has been used as a reactor. Inside the reactor another ceramic tube was inserted in order to protect the HWG from the CO atmosphere. The HWG consists of a resistively heated thin iron wire located inside the internal tube. The location of the internal tube and the hot wire can be adjusted.

The metal particles produced by the HWG are carried into the reactor with a gas flow. In the reactor, the flow of the metal particles from the HWG is mixed with the outer CO flow. Inside the reactor, CO disproportionation or hydrogenation take place on the surface of the metal particles. More details about this synthesis method can be found in [35, 36, 37, 38]. One thing that differs from this last cited publication, is the fact that in order to synthesize N doped nanotubes, an NH_3 flow diluted in the CO is utilized.

2.2.2 Boron doped SWCNTs synthesized via high vacuum chemical vapor deposition

Boron doped SWCNTs were the only materials produced *in house*. The synthesis of these boron doped SWCNTs was performed using a purpose built high-vacuum (HV)-CVD system (See figure 2.3)[8, 39]. This method allows an accurate control of all parameters that are involved in the synthesis process, such as vapor pressure of the *C/B* feedstock or synthesis temperature, among others.

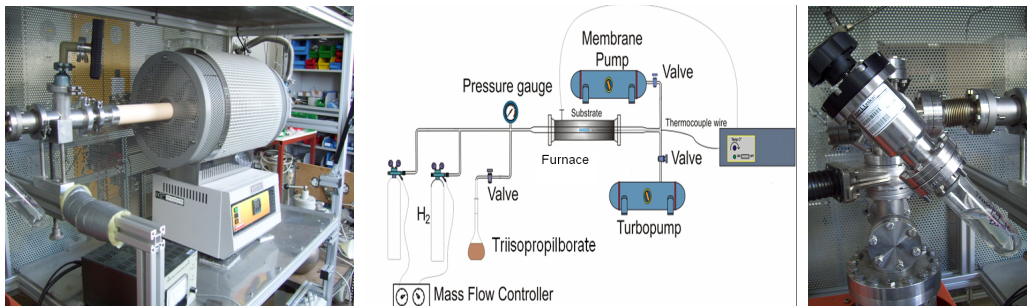


Figure 2.3: Left: Image of the purpose built system at the university of Vienna used in the B doped SWCNTs synthesis via HV-CVD. Center: Scheme of the setup[40, 41].Right:The *C/B* feedstock was conected in a purpose built container connected to the HV-CVD system through a valve that allows the release of the chosen feedstock vapor.

The experimental system (Figure 2.3) consists of an alumina tube located in the axis of a cylindrical furnace. This furnace reaches an homogeneous temperature in approximately a range of 20 cm in the center of its length. The vacuum system, connected to the alumina tube, consists of two rotary and one turbomolecular pumps, which contribute to a high vacuum of approximately 1×10^{-8} mbar. The *C/B* feedstock (Figure 2.3) and an air and hydrogen inlet are connected to one end of the alumina tube. Pressure gauges are used in the experimental system to control and avoid abrupt changes in the pressure of the synthesis chamber.

Catalysts

Dry metallic-based catalysts were prepared with different compositions. These were made of a mixture of Iron Nitrate ($Fe(NO_3)_3$) and porous Magnesium and Aluminium Oxide nanopowders [42]. The compounds were sonicated in 2-propanol (C_3H_8O) for about 2 hours. Then, they were dried removing the 2-propanol by evaporation and subsequently calcined. As final step, grinding was used to obtain a fine catalyst

powder. Every catalyst was dried at different temperatures, which are shown in the following table:

	MgO	Al_2O_3	$Fe(NO_3)_3$	Evaporation Temperature [C]
AF1		4	1	90
AF2		16	1	90
MF1	2		1	126

Synthesis process

Alumina crucibles with powder catalysts were placed inside the alumina tube. Then, the CVD reactor was evacuated with rotary and turbo molecular pumps until it reached a base pressure of 10^{-8} mbar. The temperature was increased to attain the catalyst activation temperature. The temperature increase must be done very carefully in the range from 90 to $200^\circ C$ (depending on the catalyst), to avoid contamination of the synthesis chamber. Subsequently, at $200^\circ C$, the high vacuum chamber is closed in order to supply an H_2 flow to reduce the catalyst. During this process, the pressure inside the alumina tube remained stable at 80 mbar for about 10 minutes. This time was optimized to achieve the best catalytical activity for the catalysts used in all the experiments. The SWCNTs synthesis was performed at 800° , 850° and 900° and triisopropylborate ($C_9BO_{21}H_3$) was used as C/B feedstock. Once those temperatures, the H_2 flow is stopped and the system is evacuated to the base pressure. Then, the catalyst are exposed to the feedstock vapor (between 7-9 mbar). After 10 min, the feedstock flow is stopped and the reactor is evacuated again. The system is cooled down in high vacuum. Once the system has been cooled down, the chamber is vented and the samples are removed for further characterization.

2.3 Characterization tools

2.3.1 SEM, TEM and TEM-EELS

Scanning electron microscopy (SEM)

The scanning electron microscope allows to image a sample scanning it with a high-energy beam of electrons in a raster scan pattern. The electrons interact with the atoms that make up the sample producing signals that contain information about

the surface topography and composition of the sample and other properties such as electrical conductivity. In a typical scanning microscope, an electron beam is thermoionically emitted from an electron gun fitted with a tungsten filament cathode. When the primary electron beam interacts with the sample, the electrons lose energy by repeated random scattering and absorption within a teardrop-shaped volume of the sample. The energy exchange between the electron beam and the sample results in the reflection of high-energy electrons by elastic scattering, emission of secondary electrons by inelastic scattering and the emission of electromagnetic radiation. The beam current absorbed by the sample can also be detected and used to create images of the distribution of specimen current. The raster scanning is synchronized with that of the beam on the specimen in the microscope, and the resulting image is therefore a distribution map of the intensity of the signal being emitted from the scanned area of the sample.

Transmission electron microscopy (TEM)

Transmission electron microscopy (TEM) is a microscopy technique whereby a beam of electrons is transmitted through an ultra thin sample, interacting with the specimen as it passes through. An image is formed from the interaction of the electrons transmitted through the sample; the image is magnified and focused onto an imaging device, such as a fluorescent screen, a layer of photographic film or a CCD camera.

Electron energy loss spectroscopy (EELS)

In electron energy loss spectroscopy (EELS), a material is exposed to a beam of electrons with a known narrow range of kinetic energies. Some of the electrons will undergo inelastic scattering (phonon excitations, plasmon excitations, among others), which means that they lose energy and have their paths slightly and randomly deflected. The amount of energy loss can be measured via an electron spectrometer and interpreted in terms of what caused the energy loss. TEM-EELS is capable of measuring atomic composition, chemical bonding, valence and conduction band electronic properties and surface properties. For this reason, many studies on doped nanotubes try to use this technique as the main tool to identify foreign atoms. EELS tends to work best at relatively low atomic numbers, where the excitation edges tend to be sharp, well-defined and at experimentally accessible energy losses. However, the fact that at low doping levels, the number of foreign atoms to identify is expected to be less than 0.5%at, the difficulties to use this method are still limited by instrumental problems. For this reason, it was used TEM as a spatially resolved technique and complement it with X-ray photoelectron spectroscopy as chemical analysis tool

because it provides the energy resolution lost in TEM-EELS.

2.3.2 X-ray photoelectron spectroscopy (XPS)

X-ray photoelectron spectroscopy (XPS) is a quantitative spectroscopic technique that measures the elemental composition, empirical formula, chemical state and electronic state of the elements that exist within a material. For most applications, it is, in effect, a non-destructive technique that measures the surface chemistry of any material. XPS spectra are obtained by irradiating a material with a beam of X-rays while simultaneously measuring the kinetic energy and number of electrons that escape from the top 1 to 10 nm of the material being analyzed.

A typical XPS spectrum is a plot of the number of electrons detected versus the binding energy of the electrons detected. Each element produces a characteristic set of XPS peaks at characteristic binding energy values that directly identify each element that exist in or on the surface of the material being analyzed. These characteristic peaks correspond to the electron configuration of the electrons within the atoms. The number of detected electrons in each of the characteristic peaks is directly related to the amount of element within the area (volume) irradiated.

2.4 Optical Techniques

Optical techniques have been largely used to characterize carbon nanotubes. The advantages of optics rely on both experimental and fundamental aspects. Experimentally, the techniques are readily available, relatively simple to perform, quick, and can be performed at room temperature and under ambient pressure.

Fundamentally, the optical techniques are nondestructive and noninvasive because they use the photon, a massless and chargeless particle, as a probe. Furthermore, optical experiments can be carried out at the single-nanotube level [43, 44, 45] due to the unusually high optical response of NTs, which is a consequence of the 1D confinement of their electronic structure[46]. Despite the specificity of each optical technique, the basis for the understanding of the optical responses from CNTs is common to all optical spectroscopies and can be represented by the so-called **Kataura plot**, proposed by Kataura et al. in 1999 [13].

2.4.1 Raman Spectroscopy

Resonance Raman Spectroscopy (RRS) is a characterization technique, which is widely used due to its versatility [11]. It is non destructive method that can be carried out in and air at room temperature (see the contribution by Yamamoto et al., and the contribution by Jorio et al.). RRS, combined with other techniques and theoretical calculations, determine the population of specific (n, m) nanotubes [43]. In other words, by changing the laser excitation energies, it can be observed resonance-enhancement phenomena associated with the Raman intensity from which it can be assigned (n, m) values to individual SWNTs precisely [47]. First, it is important to understand "Raman Scattering Concepts", just to reach a successful conclusion about the physical phenomena based on the results.

Raman scattering is an inelastic scattering of monochromatic light. This process can be summarized by the electron excitation from the valence (VB) to the conduction band (CB) by absorbing a photon. The excited electron is scattered by emitted (or absorbing) phonons and then the electron relaxes to the VB by emitting a photon.

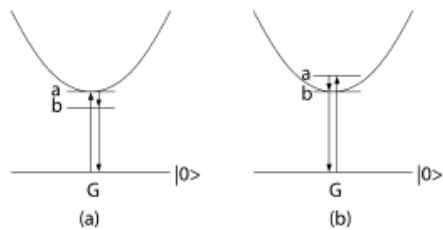


Figure 2.4: Excitation scheme of the Stokes and Anti-Stokes Raman scattering process [10].

Where phonon emission or by phonon absorption occur, the two processes are called Stokes and anti-Stokes Raman, respectively. Any molecule is excited to a virtual state and almost immediately dE-excited, with small energy difference corresponding to a change in vibrational energy.

An important concept in RRS is the exciton picture in which a photoexcited electron and hole pair is combined into an exciton. In semiconductor physics, the exciton normally has a binding energy on the order of a few meV and is observed only at a low temperature. However, for one-dimensional (1D) materials, the exciton binding energy (0.30.5 eV) is much larger than the thermal energy kBT at room temperature and thus exciton effects can be obtained even at room temperature. Because of the localized wavefunction of an exciton, the intensity of the optical process is enhanced significantly, and thus, Raman spectroscopy in SWNTs is dominated by excitons from photoexcited electronhole pairs.

Figure 2.5 shows an overview of the typical features appearing in a Raman spectrum of a SWCNT [48]. The well-defined frequency features, can be identified follows:

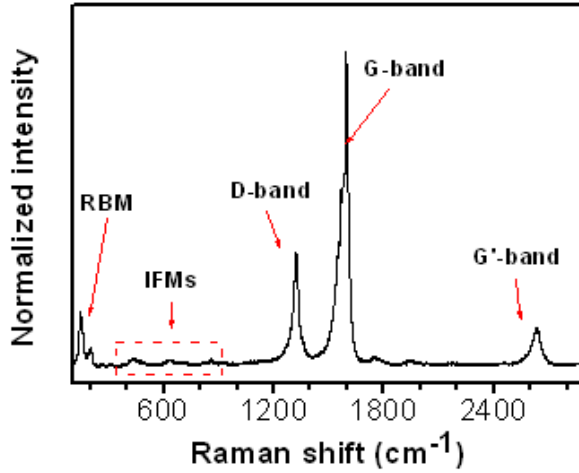


Figure 2.5: Raman spectrum from SWCNTs. Here are depicted the RBM, D, G and G' bands, which are the main observable features in this kind of spectrum.

The radial breathing mode

These are the features appearing between 100-400 cm^{-1} . The radial breathing mode (RBM) is associated with the vibrations of the carbon atoms, specifically to the coherent vibration of the C atoms in the radial direction, as if the tube were breathing. The RBM spectra have a special importance because they are a footprint of nanotubes, which does not appear for other carbon systems and it is directly dependant on the CNT diameter.

These features are unique in CNTs and occurs with frequencies ω_{RBM} between 120 and 350 cm^{-1} for SWCNTs for diameters in the range of $0,7 \text{ nm} < d_t < 2 \text{ nm}$. There is an empirical equation that provides us a proportionality relation between the frequencies and the nanotube diameter.

$$\omega_{RBM} = \frac{A}{d_t} + B \quad (2.4.1)$$

A takes into account the force between C-C bonds. Its value is 234 cm^{-1} , which was estimated by Dubax and Kresse [49]. And B is an environmental factor, which is experimentally determined. It is then easily inferable why the RBM dependence between the frequencies and the SWCNT diameter is specially used for the characterization of the diameter distribution in a nanotube sample. The Raman spectra in the RBM region for a sample composed of an ensemble of different nanotubes chiralities is strongly dependent on E_L because for each value of E_L , the optical transition energies for different CNTs are in resonance with different excitation energies. Therefore, the

intensity of the RBM for these NTs is resonantly enhanced.

G Band

The intense peak between 1500-1600 cm^{-1} is the so-called G-band, which is associated with the highest frequency optical phonon mode at the Γ point in the Brillouin zone [50]. The G Band is composed by a set of modes called tangential modes (TM), which is identified with an in-plane tangential optical phonon involving the stretching of the bond between the two atoms in the graphene unit cell. In NTs, it is composed of several peaks originating from the quantum confinement of the wave vector along the circumferential direction, and the zone folding of the graphite Brillouin zone into de SWCNTs Brillouin zone. These phonon modes have the symmetries $A(A_{1g})$, $E_1(E_{1g})$ and $E_2(E_{2g})$ originate from the first-order Raman process.

In the G band Raman spectrum, the G^- and G^+ components can be observed. These two features are associated, respectively, with vibrations of the carbon atoms along the circumferential direction (TO phonon) and along the nanotube axis (LO phonon). The G^- feature is strongly sensitive to whether the nanotube is metallic or semiconducting [51]. Due to the electron-phonon interaction, the phonon mode frequency at a certain wavevector is downshifted for one of the two G-modes. It is important to note that the assignment for TO and LO phonon modes in metallic SWCNTs is opposite to the one in semiconducting tubes [52].

D band

The *disorder-induced* band appearing between 1100-1300 cm^{-1} , is called the D-band. This is originated from a double resonance process, induced by the presence of amorphous carbon or by symmetry-breaking defects in the SWCNT structure [53].

The D band represents a defect induced mode from the zone boundary. It originates from phonons close to the K point of the graphite Brillouin zone and becomes active in NTs due to the presence of defects, such as impurities or missing atoms, among others. There is a strong dependence between E_L and the frequency, which is caused by a softening of the LO phonons near the K point due to the electron-phonon coupling. The dispersive behavior of this band is explained by a double-resonance process involving a phonon and a defect [53, 54, 55]. In this process, an electron-hole pair is created when the incident photon is absorbed. After that, the electron is scattered by a phonon (or a defect) with wavevector q and scattered back by a defect (or phonon) with wavevector $-q$, recombining with the hole and emitting a scattered photon.

G' band

Approximately at 2600 cm^{-1} is located the G' band, which is the overtone of the D-band. This feature is also observable in highly oriented graphite. The G' band is the most intense feature in the second-order Raman spectrum of SWCNTs. This band originates from a double resonance process involving two phonons. Basically, the G' band is a single Lorentzian feature, where two features can also be observed in SWCNTs (Figure 2.6)[56]. The presence of two peaks in this band indicates the resonance with two different van Hove singularities, one in resonance with incident photon and another in resonance with the scattered photon (anti-Stokes and Stokes process).

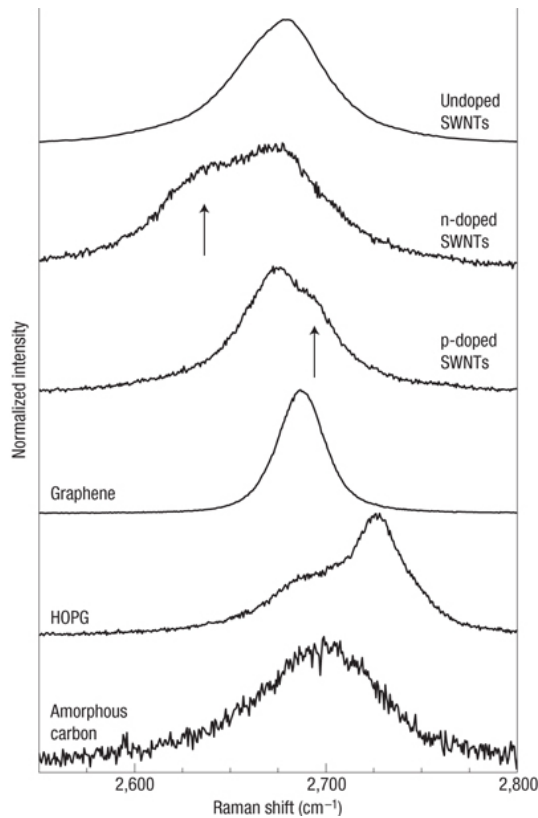


Figure 2.6: This figure has been reproduced from [57] and it depicts the G' band for different carbon materials. These spectra were measured at room temperature with the 514 nm laser line. In comparison with the spectrum of pristine SWCNTs, the n- and p- doped SWCNT Raman spectra (via substitutional B and N atoms) show a new peak at higher and lower frequencies, respectively.

In the case of metallic NTs, the two peaks observed in the G' band are caused by an anisotropy of the phonon dispersion around the K point, known as the phonon trigonal warping effect [58]. In the case of doped SWCNTs, Maciel et al. [57] work should be mentioned. They suggested that N doped SWCNTs exhibit a lower frequency G' Raman peak, since one extra electron causes an electron and phonon renormalization

near the defect site. On the other hand, in B doped SWCNTs, the shift of the G' goes to the opposite direction due to the presence of a hole.

Intermediate Modes

In the middle of the RBM and the D-band ($600\text{-}1100\text{ cm}^{-1}$), there is a zone of several low intensity features called intermediate frequency modes (IFMs), which are associated with a second-order Raman processes. These features are still the focus of some research since their interpretation and assignment are still an open issue.

2.4.2 Optical absorption

From the experimental and analytic point of view, optical absorption (OA) is the simplest optical technique. OA can be used easily to show the presence of SWNTs in the sample [59] from the observation of absorption peaks related to the first and second optical transition from semiconducting tubes, and the first optical level of metallic tubes. For higher optical levels, the optical absorption response gets blurred due to the absorption by s-bonded electrons. OA can also be used to characterize the metal vs. semiconducting SWNT separation process, or just the separation of tube bundles into isolated SWNTs.

Figure 2.7 shows the relation between the OA profile of a SWCNT sample and its corresponding Kataura plot. Basically, light will be absorbed when in resonance with E_{ii} values for the (n,m) nanotubes in the sample. The resonance width depends strongly on sample environment, and the broad peaks observed in (Figure 2.7) are actually related to groups of unresolved absorption profiles for different (n,m) SWNTs with similar E_{ii} values. The presence of groups absorbing at similar frequencies can be used, for example, to characterize the separation between metallic and semiconducting tubes. The (n,m)-dependent OA spectra can be resolved when a sample has a small diameter distribution, and this approach is effective mainly for smaller-diameter tubes. For larger-diameter tubes the number of different (n,m) with similar E_{ii} increases. As a rule of thumb, when the bands in the Kataura plot are well separated from one another, the distinction between one $(2n + m)$ family and another can be effectively done, and for small diameter tubes, individual (n,m) can be identified from the absorption spectra. Comparative analysis performed on different samples can be made accurately. For an absolute population analysis, however, like defining how many per cent of one given sample is metallic and semiconducting, or is related to a given (n,m) species, it is important to know the optical absorption efficiency as a function of (n,m), E_{ii} and the environment.

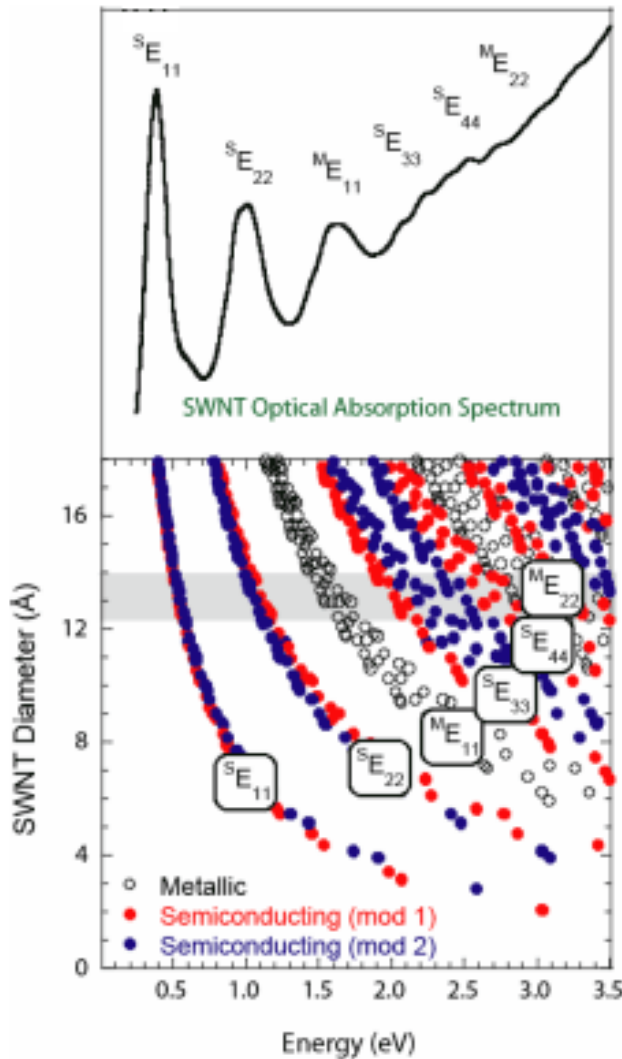


Figure 2.7: Above: Optical absorption spectrum for SWCNTs. Below: Kataura Plot of the electronic transitions for SWCNTs. The spectrum is a convolution of the diameter distribution for the sample [60].

2.4.3 Photoluminescence

Among the optical techniques, photoluminescence has the strongest signal. Similar to Raman spectroscopy, photoluminescence can be used to measure the effect of temperature, pressure, strain, etc., on the E_{ii} optical levels of isolated tubes, as well as for the (n,m) population analysis. While Raman has a unique signature (E_{ii}, ω_{RBM}) for each (n,m) tube, photoluminescence excitation spectra [61] provide another unique signature, that is obtained by measurement of the (E_{22}, E_{11}) for each specific (n,m) tube. Such an experiment is shown in (Figure 2.8). Each darker gray dot represents a strong emission at E_{11} , stimulated by a prior strong absorption at a higher E_{ii} level, for one specific (n,m) species. The (E_{22}, E_{11}) pairs can be well established when

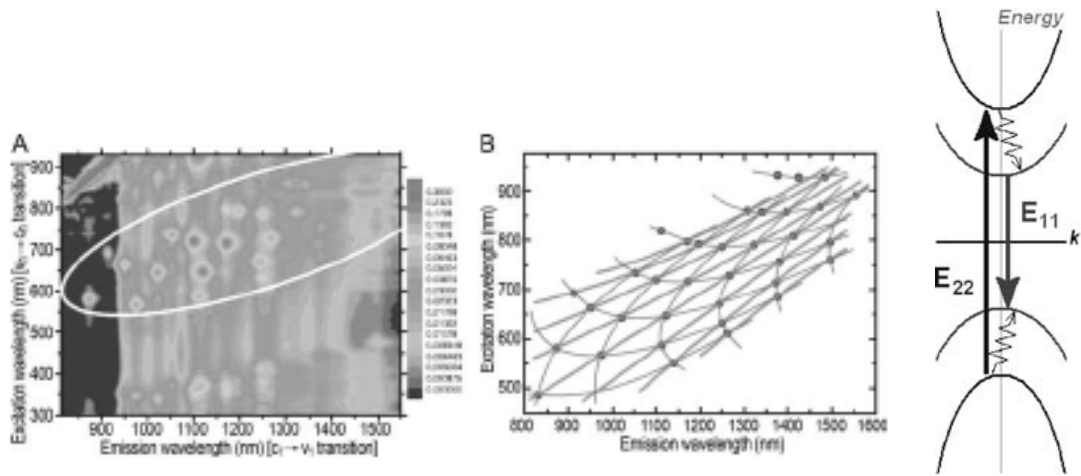


Figure 2.8: Left: Photoluminescence excitation map. Each darker gray dot represents the absorption at E_{ii} ($i > 1$) on the Y-axis and emission at the E_{11} on the X-axis for a given (n,m) SWNT. Right: Schematic of the PL pattern formed by the $(2n+m)$ and $(n-m)$ SWNT families within the E_{22} absorption and E_{11} emission peaks (contained within the white ellipse)[62]

a full photoluminescence excitation map is performed, like in (Figure 2.8), and they show nice $(2n+m)$ and $(n-m)$ family patterns that yield the (n,m) assignment for each PL feature[11, 62]. If using only a small set of excitation laser energies, the (n,m) population can be rapidly extracted by PL-line shape.

One strong limitation, however, is the sample preparation. Nanotubes contained in bundles do not luminesce, nor can metallic tubes within a sample be measured. The photoluminescence signal from SWNTs can only be measured on isolated semiconducting SWNTs. Isolated SWNTs should be grown suspended on Si/SiO₂ substrates, crossing over lithographically prepared trenches, using a CVD method. Alternatively, sonication of SWNT-bundle samples in solution also produces isolated SWNTs, and wrapping each nanotube with surfactants guarantees that tubes previously separated by sonication will not rejoin subsequently. In the following section, it has only been performed photoluminescence studies of B-doped SWCNTs because of the amount of sample that is required to do treatments prior to any measurement.

2.4.4 Equipment used in the thesis

For Raman spectroscopy characterization were used the spectrometers in-house:

FT-Raman spectrometer

An **FT-Raman spectrometer** (IFS100 Bruker FT-Raman spectrometer) with a *Nd : YAG* laser with a wavelength of 1064 nm. This instrument has a front measurement chamber and an attached Raman microscope. It have been used a resolution of 2 wavenumbers for our measurements.

Dilor xy triple monochromator spectrometer

A **Dilor xy triple monochromator spectrometer** which allowed us to perform multi-frequency Raman characterization. This spectrometer can be operated in either in normal resolution (NR) or in high resolution (HR). The resolution depends on the wavelength of the laser and the chosen mode, but in the case of HR mode, a 0.5 nm wave numbers of precision can be reached. The lasers used in the measurements were an *Ar + /Kr+* ion laser (Spectra Physics, model Stabilite 2018) and a *He/Ne* laser (Spectra Physics, model 127). With both lasers, a range of discrete lines, between 488 and 632 nm excitation wavelengths can be used, which favors our purpose to perform a multifrequency analysis of our samples with the Raman spectroscopy technique.

Labram HR

Additionally, a **Labram HR** with a coupled HeNe Laser is available at the LQDS group at the University of Vienna. This spectrometer provides a high spectral resolution and fast acquisition times.

FT-IR spectrometer

VERTEX 80v vacuum FT-IR spectrometer was used to measured optical absorption on the samples. This instrument is based on the actively aligned interferometer, which provides PEAK spectral resolution. It is equipped with optical components to cover the spectral range from the far IR, or terahertz, through the mid and near IR and visible and up to the ultraviolet spectral range and its configuration provides apodized spectral resolution of better than 0.2 cm^{-1} .

Spectrofluorometer

For the photoluminescence measurements, the **NanoLog spectrofluorometer** was used. It detects fluorescence in the near-IR from 800 to 1700 nm (optional multi-channel detection to 2 m, single-channel detection to 3 m), with visible and UV options possible. With the NanoLog comes specially designed software ideal for classifying SWNTs, performing energy transfer calculations, and saving custom routines and instrument layouts. A complete spectrum can be scanned as fast as a few milliseconds, and a full excitation-emission matrix scan can be taken in as little as seconds.

XPS, TEM, EELS

Some of the figures and spectra shown here have not been done in house but they are required for the proper interpretation of the obtained results. In particular, determining the changes in the spectra recorded in work, related to the introduction of dopants, requires of methods that allow identifying amounts and sites where heteroatoms are introduced.

XPS was done at the IFW-Dresden in Germany using a PHI5600 spectrometer equipped with a monochromatic AlK α source (1486.6 eV) with an overall spectral resolution of 0.5 eV.

TEM and electron diffraction were used to study the morphology and the structure of the N-doped SWCNTs from Ferrocene Reactor. The Philips CM200-FEG Transmission Electron Microscope (TEM) was used for high resolution structure determination, which operated at 80 kV. The microscope is equipped with a slow 1kx1k CCD camera (Gatan 794).

EEL spectra were recorded using a VG-HB501 dedicated scanning transmission electron microscope (STEM) instrument equipped with a cold field emission gun (FEG). It was operated at 100 keV with an energy resolution close to 0.7-0.8 eV in the core-loss region. Convergence angle on the sample was 15 mrad and the collection angle, 24 mrad. The spectroscopic information was obtained using a spectrum-imaging (SPIM) acquisition mode [63], and for the spectra acquisition was used a slightly defocused electron probe, which was scanned in a small area of few nm².

SEM

SEM images were taken in-house with a Zeiss Microscope.

Chapter 3

Results and Discussion

The following chapter summarizes the results obtained in this thesis. The Raman spectroscopy technique was used for all the available samples. The particular interest is the comparison between the variations of the Raman features characteristic of SWCNTs upon incorporation of N heteroatoms through the three methods mentioned in the precedent chapter. Additionally, the B-doped SWCNT samples synthesized by HV-CVD were also exhaustively analyzed by Raman.

3.1 N doped nanotubes

3.1.1 Overall Morphology

As already mentioned in the previous chapters of this thesis, in this work have basically been analyzed two types of samples of CNTs doped with N during synthesis (HWG and Ferrocene Reactor) and one based on a post synthesis method (ion implantation). It is clear that the morphology of these kind of samples is significantly different from one to the other.

This morphological description can start from the N-doped material synthesized by the hot wire generator (HWG) and the Ferrocene (FeCp₂) methods shown in figure 3.1. The NMG group in Aalto University in Finland developed a method with which they are able to collect nanotubes directly onto filters making use of vertical reactors. The image on the left side of 3.1 shows a filter with a dark gray color arising from the nanotube material there collected. Varying the times for collection,

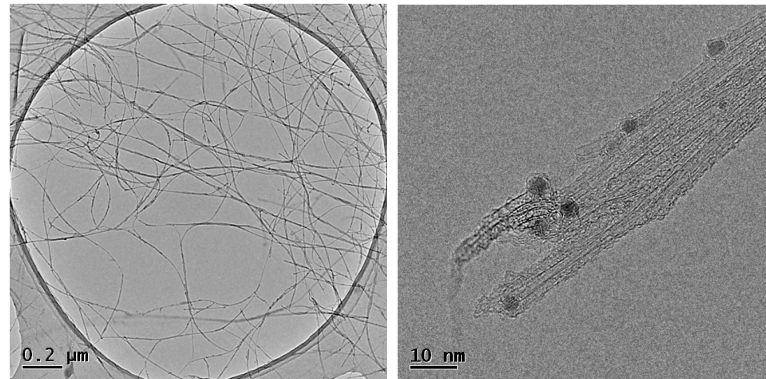


Figure 3.1: Low magnification SEM micrograph of the B-doped material as grown. The inset image shows a closer inspection to bundles of nanotubes. Images provided by T. Susi (NMG Aalto University)

it is possible to have films with different thicknesses that can easily be transferred to different substrates for further applications. Both kinds of nanotubes (FeCp2 and HWG material), look similar when deposited on top of the filters. One of their main differences is the production rate. The ferrocene reactor produces much darker films (more nanotubes) in significantly lower time. When this material is more closely inspected as seen in the middle image of 3.1, it can be seen that the material collected on a TEM grid appears relatively clean. This is raw material which does not undergo any purification process, which in several cases can be extremely advantageous. It was used to conveniently transfer the nanotube films onto conducting substrates when required for some of the spectroscopic techniques.

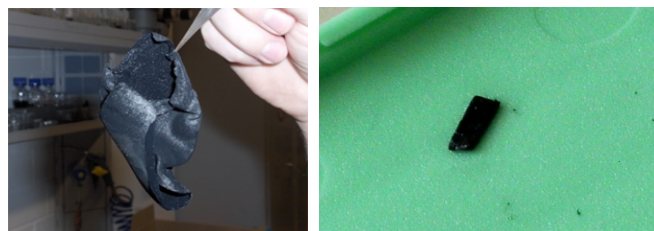


Figure 3.2: Left: Photograph showing the raw product of pristine SWCNTs produced by laser ablation. Right: a 25 mm² bucky paper of SWCNTs after ion implantation.

As for the ion implanted samples, the starting material is a buckypaper of laser

ablation nanotube material. The left photograph on figure 3.2 shows the raw material corresponding to laser ablation can be produced in large amounts in one run. Specifically, the nanotubes synthesized by this technique, which were provided via collaboration with the IFW-Dresden, were synthesized using non-magnetic catalysts and then purified and filtrated to pack it in a bucky paper fashion. The bucky paper was cut in small pieces as shown in figure 3.2 introduced into the high vacuum chamber to perform the implantation. The product of this process is shown in the right photograph. It is worth mentioning here that laser ablation is a technique able to produce bulk amounts of SWCNTs with a very narrow diameter distribution, which will be discussed in more detail in the following section.

3.1.2 Analysis of mean diameter and diameter distribution of doped nanotubes

All the samples were characterized by Raman spectroscopy with the different spectrometers described in the previous section. All the features related to SWCNTs that usually appear in a Raman spectrum were recorded. In order to determine the range of diameters and their distribution in the samples on the bulk, Raman spectroscopy was done in a multi-frequency range of wavelengths to cover most of the possible tubes in resonance with the specific laser lines.

It is observed that all types of samples exhibit distinctive features, for that reason, the radial breathing mode will be firstly focused as part of the structural characterization.

N-doped SWCNTs from the Ferrocene Reactor

For these kind of N-doped nanotubes the synthesis was optimized at 1000C by the group who provided with this material. Raman spectra, were recorded for samples synthesized at the mentioned temperature with 0, 250 and 650 ppm NH_3 diluted in the C. First, the D and G band Raman region in figure 3.3 shows a multifrequency study on all the samples recorded with the following excitation wavelengths: 488, 514, 568 and 632 nm. It can be seen that the I_D to I_G intensity ratio increases with the increase of ammonia used during the synthesis process. This ratio is frequently used in nanotube metrology to determine the crystallinity of the samples. However, the changes in the phonon modes responsible for the G and D band features can also have a contribution from the dopant distribution along the individual tubes and the bundles. For this reason, it is not taken this as a conclusive argument to judge the quality of the SWCNTs.

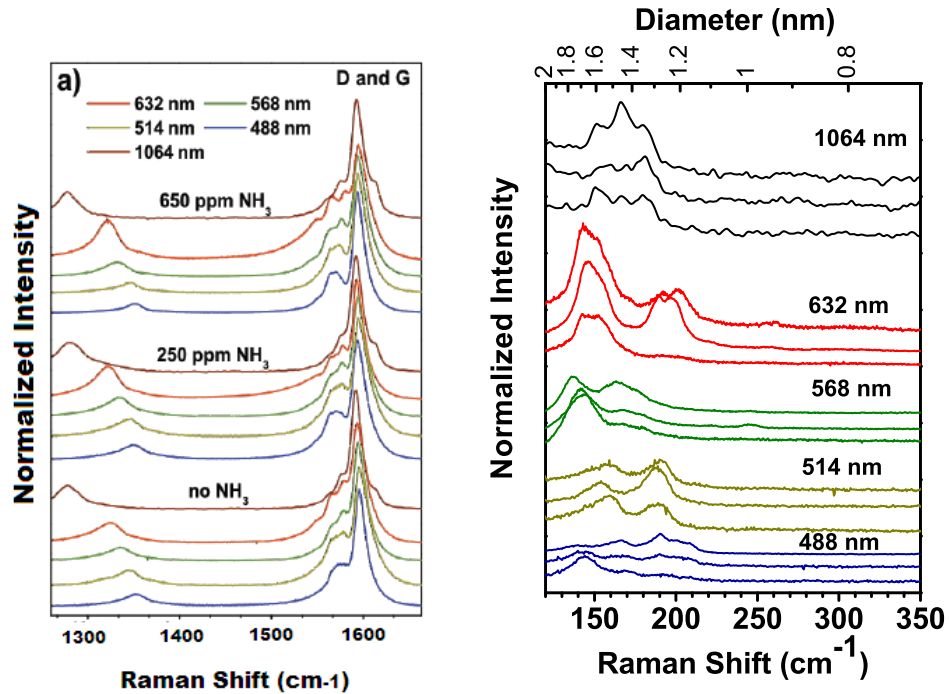


Figure 3.3: Left: D and G band multi-frequency spectra. These were recorded for the 488, 514, 568 and 632 nm excitation wavelengths. Right: Multifrequency Raman response in the RBM region.

Further analyzing the morphology of this bulk material, the RBM region, recorded for the same samples various laser lines, is focused. With this MF study the nanotubes diameter distribution within the sample can be indentified. Figure 3.3 shows on the left side the RBM region recorded for all samples with the FT-Raman spectrometer, whereas the graphic on the right side shows the MF RBM study recorded with some of the laser wavelengths chosen from the He-Ne laser. These nanotubes have large diameter which are in the typical range for CVD tubes (1.2 to 2.4 nm). Comparing this study with the optical absorption spectra and with an extended Kataura plot done in the same material. Those results (not shown here), were used to approximate the RBM spectral region. The authors approximate the mean diameters of the nanotubes in the 0, 250 and 650 ppm NH_3 samples and the diameter values obtained are 1.5 ± 0.2 , 1.6 ± 0.3 and 1.4 ± 0.2 nm, respectively.

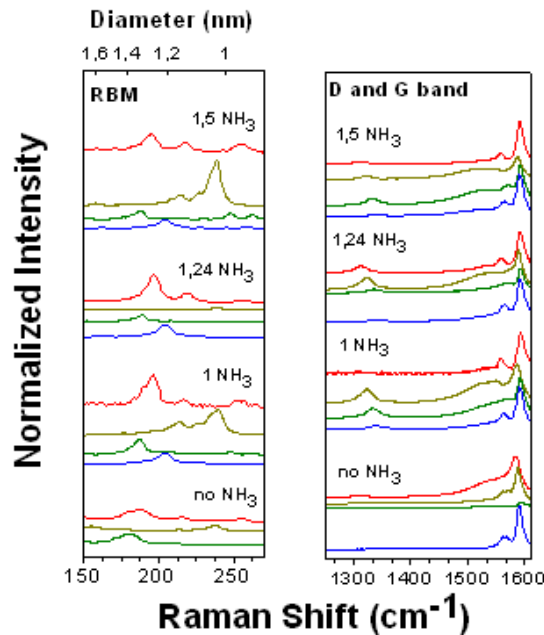


Figure 3.4: Left: RBM response for N-doped nanotube samples synthesized with the HWG method, recorded with different excitation wavelengths. These samples were synthesized with 0, 1, 1,24 and 1,5 ppm NH_3 with the simultaneous CO flow to produce doped nanotubes. The Raman spectra were recorded with the 488, 514, 568 and 632 nm laser wavelengths. Right: The D and G bands recorded for the same samples with the corresponding laser excitation wavelengths are shown.

N-doped SWCNTs from the HWG Reactor

As it was cited above, the nanotubes from the HWG reactor are similar to the FeCp2 reactor material with an overall inspection. However, differences have been reported for pristine carbon nanotubes synthesized using merely CO as carbon precursor in the growth process. For pristine SWCNTs, the diameters of the SWCNTs made on the FeCp reactor are larger [36] but the growth rate is much higher. In that case, the choice of growth method is linked to the final use interest. Another crucial difference is related to the byproducts present in both types of materials. In the case of the HWG samples, it has been observed that for pristine C nanotubes, it is possible to obtain relatively clean material with very few catalytic remaining, whereas the FeCp2 material contains higher amounts of additional carbonaceous byproducts. Now analyzing the case where doped material is aimed, NH_3 has been introduced in the synthesis process. For the ferrocene reactor, it has been reported that NH_3 seems to be working as an etching agent which not only can dope the nanotube-material, but also allows obtaining a cleaner final product.

Again, the material produced at optimized synthesis conditions was used. The Raman spectra recorded for samples synthesized at 890°C with 0, 100, 200 and 300 ppm NH_3 are shown in (Figure 3.4), which contains the features characteristic of SWCNTs. The RBMs are shown on the left panel. The right panel of the same figure

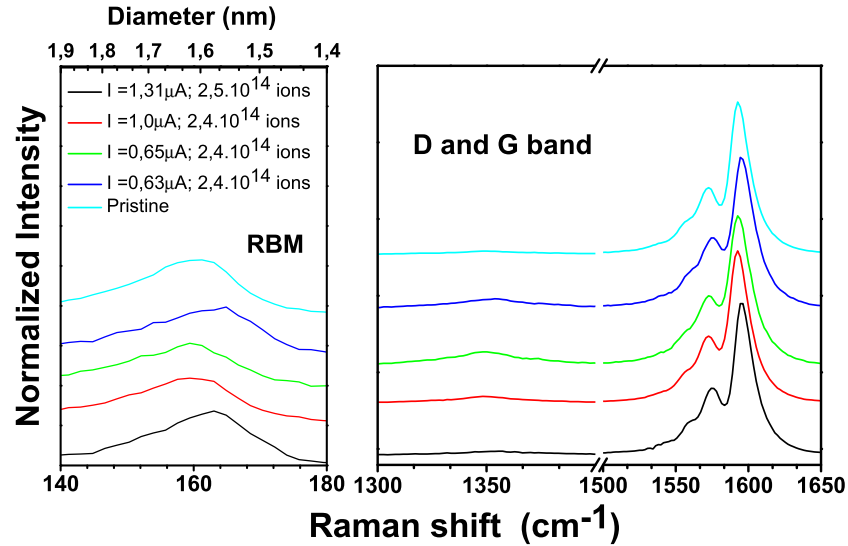


Figure 3.5: For different dose and current, it was recorded the Raman response for the 487 nm excitation wavelength. Here, it can be seen the RBM, which were used to estimate the diameter distribution for this kind of samples. It is also shown the D and G bands.

shows the disorder-induced Raman peak and the G band, which correspond to SWCNTs. It is observed no downshift in the G band, contrary to what has been reported for N-MWCNTs. It has been reported that for N-doped nanotubes, changes in the G band are likely to occur due to a change in the diameter distribution. However, it is not observed such change. The D band has also been reported to change but it cannot be seen any intensity changes.

The main difference in these samples in comparison to the FeCp2 ones is related to the nanotube diameters. The material grown in the HWG apparently promotes the growth of larger diameter tubes upon the incorporation of NH_3 in the synthesis. However, again, this is not necessarily related to the dopant concentration which could be present in the wall of the nanotubes. This would have to be correlated with the dopant concentration and bonding environments inspected by analytical methods as it will be mentioned later in this same chapter.

N-doped Laser Ablated SWCNTs and Ion Implantation

Xu et al. [28] proposed N ion implantation post growth in commercial nanotubes obtained by different techniques. These experiments are performed in a UHV chamber allowing in situ oxygen treatment, annealing, and latter implantation of low voltage N_2^+ ions. Although an exhaustive study of the material postdoping has been made by XPS, with consistent line-shape analysis, a high percentage of N to C bonding in a tetrahedral sp^3 configuration was detected. This confirmed that the technique inevitably produces disorder in the C network. Further morphological studies were required to differentiate doped material from other carbonaceous amorphous by-products. In this thesis a Raman spectroscopy analysis was performed, which was lacking in that study to understand better the doping feasibility via ion implantation.

As it was mentioned before, the laser ablation SWCNTs were ion implanted with different doses and current. The spectra shown in figure 3.5 were measured for samples with different ion implantation rate with a 487 nm excitation wavelength using Raman spectroscopy. The RBM, D and G bands for each sample are depicted. In this case it is very important to keep in mind that the starting material is the same and any change in the spectra can be directly related to the implantation rate. In this case we do not show a multifrequency analysis but only try to identify changes on samples that had identical spectra before irradiation. In the RBM spectra show a well-defined range of diameters between $\sim 1,7$ and $1,6$. If the pristine is considered (light-blue line), it can be seen a slightly shift (of ~ 2 wave numbers) to higher frequencies.

The D band is relatively small and placed with a peak at ~ 1350 wave numbers, which confirms the typically high crystallinity of the laser ablation nanotube material. The G band presents a small shift (about ~ 2 wavelength) to higher frequencies in comparison with the pristine SWCNTs. It is noted that there is a peak close (about ~ 10 wavelength) to the higher peak of the G band, which remain in the same position from the reference. This peaks could be associated with the two components of the G band (G^- and G^+), but in this case, more information is needed to fit correctly the spectra and to draw accurate conclusions about it. Thus, this will not be developed in this work.

3.1.3 N content and bonding environment on samples

The determination of the nitrogen content and bonding environments has been developed as a parallel project to this master thesis. The different nanotube samples have been studied with EELS in TEM as a locally resolved technique, as well as XPS as a bulk probing method. Those detailed analysis are not presented in this thesis but the

values and bonding environments will be used for comparison purposes taking into account the properly corresponding citations.

First, in the case of the Ferrocene reactor nanotubes, XPS was used as probing method. The maximum nitrogen content in all the samples was around 1%at. However no consistent increase or decrease of the nitrogen substitutional environment was observed related to the synthesis parameters. This is not a negative point but a disadvantage which implies that there is a possibility to grow directly nanotube films using NH_3 in vertical reactors, where the overall nitrogen content can be tuned but controlling the bonding environments in such a system turns into a very difficult task.

On the other hand, the material from the HWG was studied with XPS as well as with TEM-EELS. The nitrogen content in these samples has been estimated around $1.7 \pm 0.8\%$ at in the highest concentration regions. On the marked area of the bundle of N-SWCNTs, synthesized at 1000C with 625 ppm NH_3 , was recorded the EELS spectrum (Figure 3.6), which is the sum of 5 EEL spectra with an acquisition time of 20 s each. The features near of the edge of the C-K edge consist of a π^* peak at 285eV and σ^* band starting at 292eV , which suggests that the SWCNTs are well crystallized. The peak at 398eV could be associated with pyridine-like configuration [64, 63, 65]. The TEM observations showed that the incorporation of N into the carbon network is inhomogeneous (from 0 to 3at.%) and the mean nitrogen content is estimated to lie around 1.7at.%.

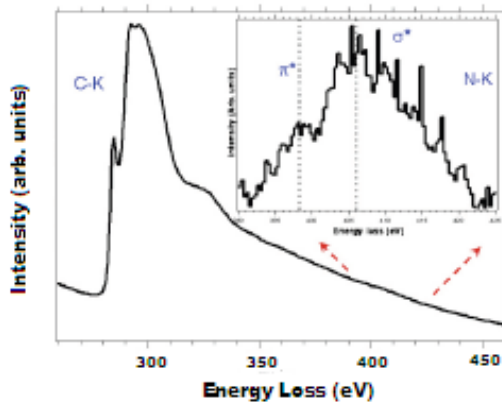


Figure 3.6: An EEL spectrum showing the C- and N-K edges appearing from a N-doped SWCNT bundle after an acquisition time of 20s each. The sample used for this was synthesized at 1000C with 650 ppm NH_3 , shown in the bright field micrograph. The inset shows a magnification of the N-K edge after background subtraction. This image has been modified from T.Susi et al. (PSSb 2010).

Finally, in the case of the ion implantation samples, it is still necessary to perform a follow up morphological study via local probing methods. Although changes in the Raman features of the samples can be observed, it is still necessary to perform more studies, which will be done as a future perspective. As already mentioned in the previous chapters of this thesis, in this work two types of samples of CNTs doped with N during synthesis have been analyzed (HWG and Ferrocene Reactor) and one based on a post synthesis method (ion implantation). It is clear that the morphology of these kind of samples is significantly different from one to the other.

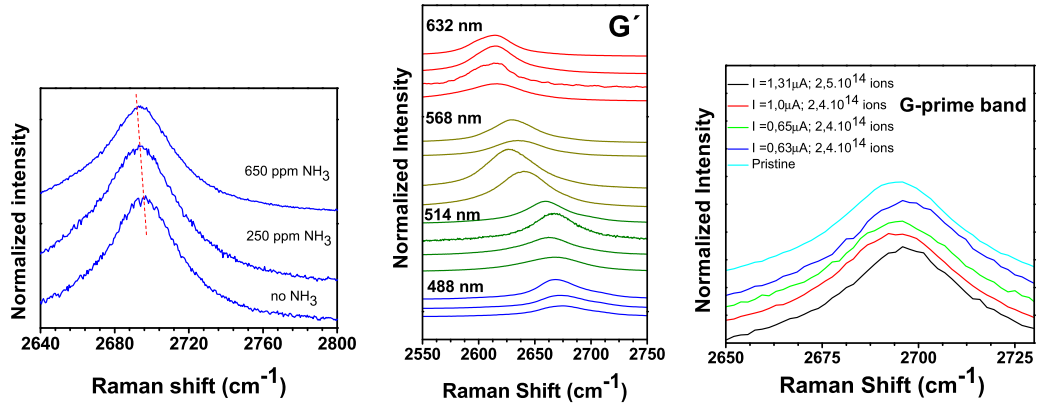


Figure 3.7: Left: G' band spectra recorded for the 488 nm excitation, measured for samples synthesized at 1000° C with 0, 250 and 650 ppm NH_3 . Right: G' zone of the multi frequency raman response for samples with different NH_3 concentration. Samples were recorded for 488,514, 568 and 632 nm laser line. (third) G' band for samples with different implantation dose and current, recorded for 488 nm wavelength.

The graphic in 3.7 summarizes the spectra recorded in the G band region for all N doped samples. The changes of the G' band in the samples due to doping were proposed in reference [57]. In the case of doped SWCNTs, the authors suggested that N doped SWCNTs exhibit a lower frequency G' Raman peak, since one extra electron causes an electron and phonon renormalization near the defect site.

In the FeCp2 reactor material, it is observed a downshift of 1.4 nm wave numbers at the center of the maximum of the G peak on the first sample synthesized with ammonia in comparison to the spectrum corresponding to the pristine material and an additional shift of 2 wave numbers in the upper spectrum, which can be attributed to the high doping level. Although there are some reports that claim the possible dependence between the RBM Raman band with the doping level [31], it is not possible to attribute this fact to the results obtained.

3.2 B doped nanotubes

3.2.1 Overall Morphology

The in-situ B doping of SWCNT was the aim of the experimental work in-house, for which the parameters towards improved growth conditions were studied. For the synthesis, catalysts with different composition were used. These compositions were detailed in the description of the synthesis process used for B-SWCNTs. Previous referential papers [39] reported the possibility of the B-doped SWCNT growth via CVD-HV, using Triisopropylborate as a C/B precursor. The temperatures used for synthesis were 800C, 850C and 900C were chosen based on the mentioned citation. It is shown that the synthesis of those kind of doped nanotubes using the mentioned precursor gives the maximum Raman response for samples formed between 790 and 890C. In this temperature range, a relatively low defect concentration is observed.

As a fast inspection method to control the samples obtained, the FT-Raman spectrometer was used. It was observed that using magnesium oxide supported catalyst it was possible to grow nanotubes relatively easily.

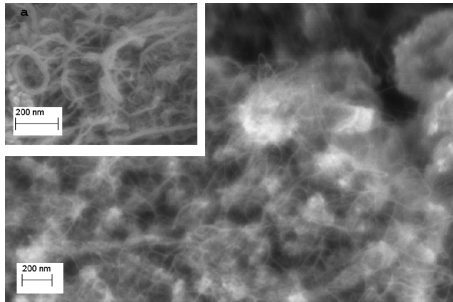


Figure 3.8: Low magnification SEM micrograph of the B-doped material as grown. The inset image shows a closer inspection to bundles of nanotubes.

A SEM image is shown in figure 3.8. White agglomerates are observed, which correspond to the remaining supporting material used in the catalysts as previously described.

It is worth noting again that the catalysts were made keeping in mind the decomposition of iron nitrate to form the metal oxide simply dissolving it in ethanol. It was observed that using higher weight percentages of magnesium oxide supporting material were ideal and favorable nanotube growth. In the same image in fig. 3.8, it is clearly seen that the nanotube bundles appear everywhere in the sample.

As part of the optimization process, a hydrogen flow at a constant pressure of 80 mbar and at a temperature of 200C, for approximately 15 minutes was introduced in the synthesis process. The hydrogen flow is done to reduce the oxygen from iron oxide that forms after the decomposition of the iron nitrate [66].

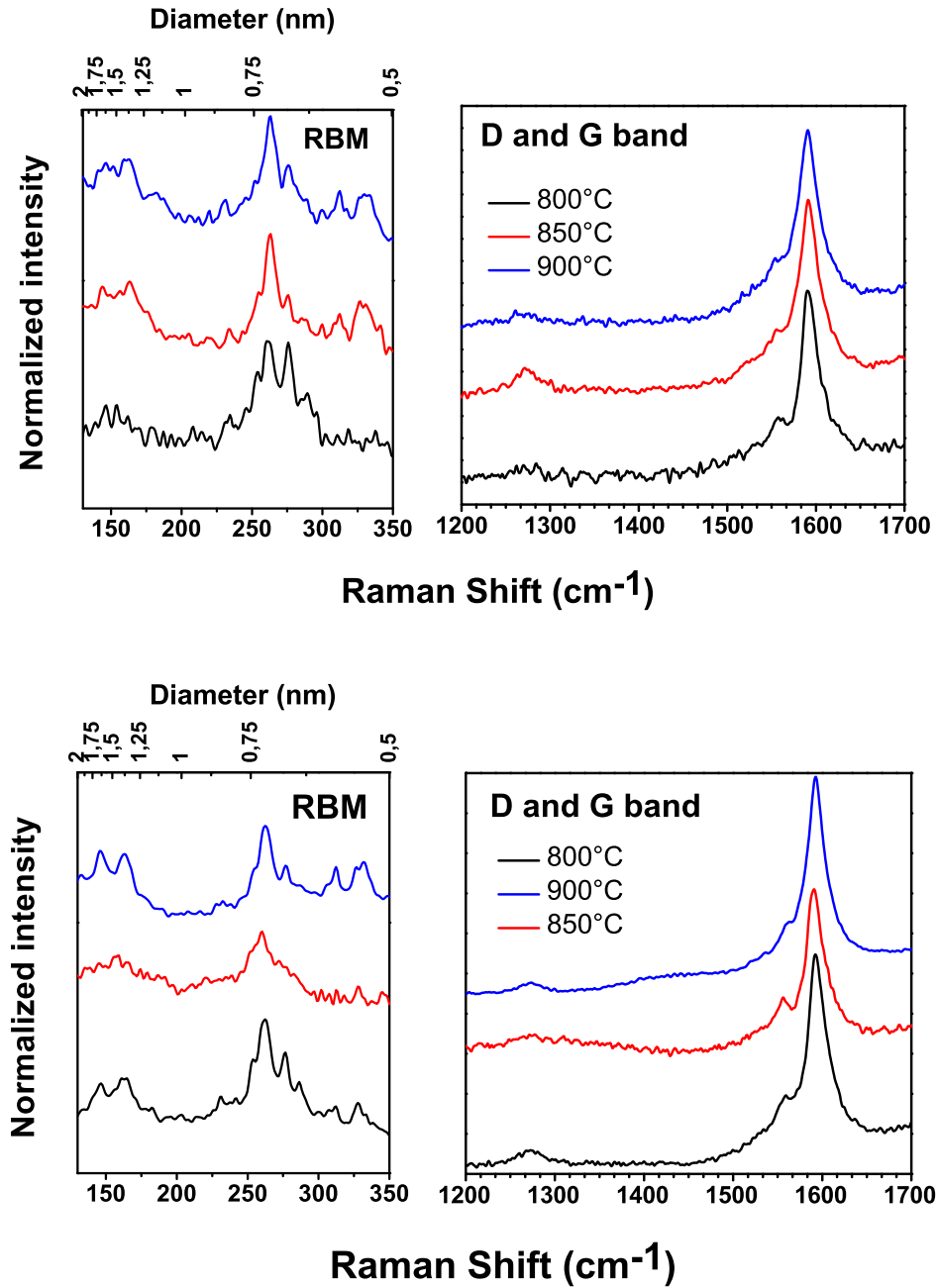


Figure 3.9: Raman spectra of the sample MF1 for the 1064 nm excitation. In the figure are shown the RBM, the D and the G bands for different temperature. Lower spectra: Raman response of the B-SWCNTs synthesized with the catalyst MF1 with hydrogen reduction. In this case, during the synthesis process, an hydrogen flow was introduced to extract the oxygen from the catalyst surface.

3.2.2 Optical properties, defects concentration and doping level from Raman

The spectra were recorded with the FT-Raman spectrometer with the 1064 nm excitation wavelength for all samples are shown in figure 3.9.

The RBM spectra can be seen very clearly and show a peak at ~ 263 wave number, which remains constant for all the temperatures. The average diameter of the samples, was estimated around $\sim 0,8nm$. The D to G ratio is very low. There are no changes in the D band, which is located ~ 1270 wave numbers, as the RBM, the G band always appear in the same position for all the temperatures with a non significant alteration of intensities. This leads one to conclude that the temperature is one important parameter but not crucial for the SWCNT growth in this process.

There are no signal of intermediate frequencies modes (IFMs) but it is observed some non-typical peaks in the zone between the G and the G' bands. Those peaks appear to be coupled (as a shifted peak) and remains in the same position for all the temperatures.

If the spectra measured at 850C is considered as a reference (red line), the G' band, for the others spectrum, presents a slightly shift (of ~ 7 wave numbers) to lower frequencies.

In (Figure 3.9) is shown the spectra for the samples when a Hydrogen flow is incorporated to the synthesis process. Here, the same features than in the other spectra are observed. However, the G' band presents a slightly shift (of ~ 3 wave numbers) to the other side (to higher frequencies) due the presence of a hole. In this case, the estimated average diameter remains the same.

The sample synthesized at 850° C, with a H_2 flow, was measured by Photoluminescence (Figure 3.10).

As the photoluminescence signal only can be measured on isolated SWCNTs, this samples was suspended on 1% w/v SDBS (4-Dodecylbenzenesulfatonic acid). Sonication of SWCNT-bundle samples in solutions was done to separate them into insolated tubes. Later, they were wrapped with surfactants to guarantees that the previously separated tubes will not rejoin subsequently.

In the photoluminescence excitation map (Figure 3.10) can be seen peaks which were levelled by black circles. This peaks correspond to the expected theoretical map for this kind of tubes. Emission from (6,5),(7,5), (7,6), (8,3), (8,4) and (8,6) are the most intense peaks. Here are shown the same chiralities as in the CoMoCAT samples.

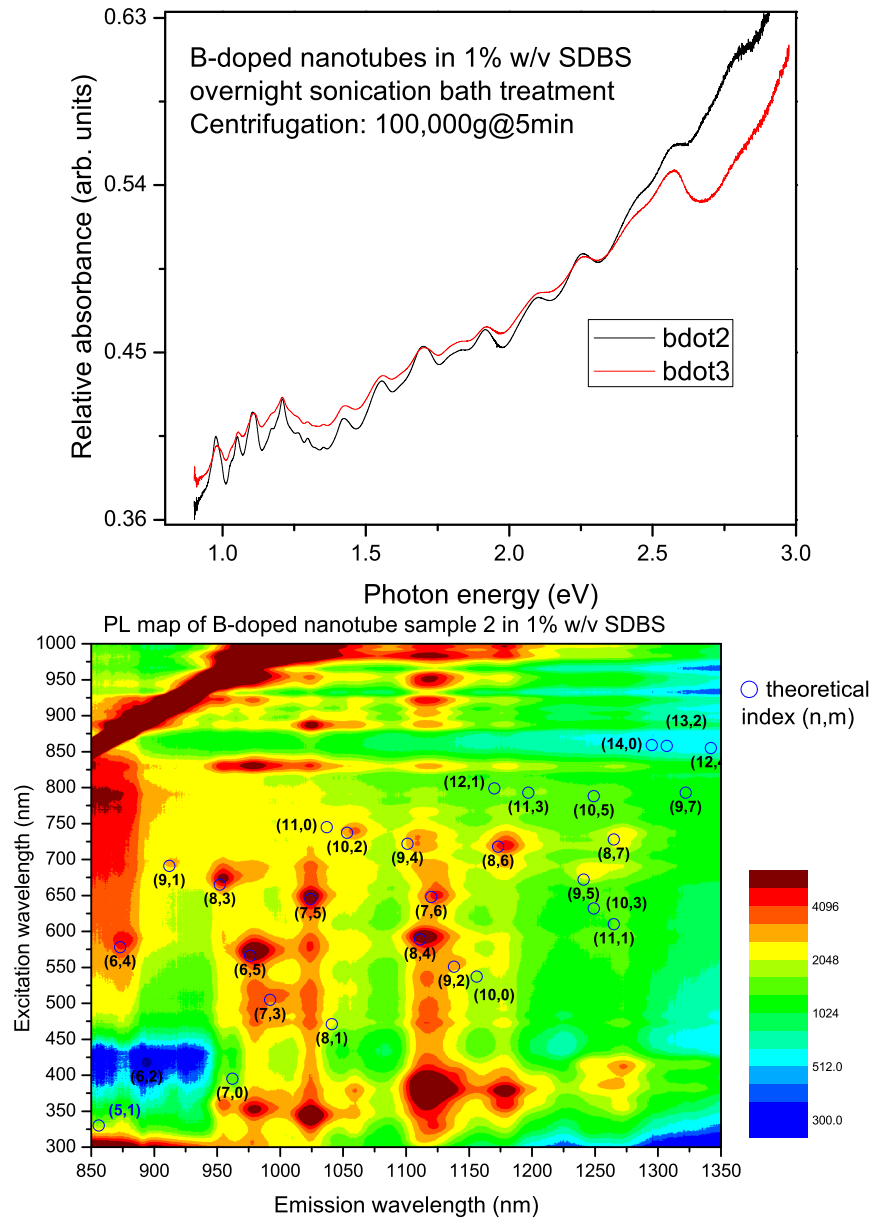


Figure 3.10: Above: Optical absorption spectrum of B-doped SWCNTs in 1% w/v SDBS, recorded after an overnight sonication bath treatment. Photoluminescence 2D spectrum for the sample, which was synthesized at 850° C.

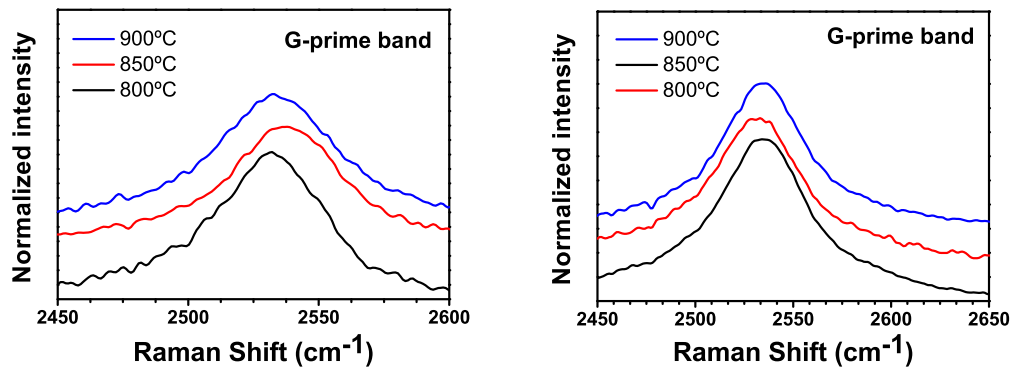


Figure 3.11: Boron doped nanotubes. In the figure, the G' band recorded for samples synthesized with diferent parameters is shown. Below, the spectra was recorded for samples synthesized with previous reduction in a H_2 atmosphere.

Chapter 4

Conclusions & Future Perspectives

In this master thesis project, an exhaustive spectroscopic study of different samples of SWCNTs doped with nitrogen have been done. The reports in the literature tend to generalize the the characterization observations regardless the material analyzed, and this is the main reason why the study here was performed as such.

Two different kinds of SWCNTs grown by two variations of CVD in vertical reactors were used. The pristine carbon nanotube-material was in principle different, and the Raman spectra corresponding to both were evidently different. Once the pristine material was compared for all of our samples, the doped material was analyzed. To a certain extent, the predicted changes in the Raman features characteristic of SWCNTs upon doping were observed. As a further study, the doping level with N in the samples should be studied in order to propose a metrology method to correlate Raman shifts with doping level.

On the other hand, samples which were doped after synthesis were studied. This is the case of the samples with ion implantation. The largest difficulty faced with this samples is to understand to what extent the method produces damage in the nanotubes and to what extent they are eventually doped. It has been used mats of SWCNTs which were irradiated with mild as well as extreme ion implantation doses. Given the fact that a buckypaper was used, there was the option to analyze both sides of the material post doping.

Bibliography

- [1] M.S. Dresselhaus, G. Dresselhaus, and P. Avouris. *Carbon Nanotubes: Synthesis, Structure, Properties, and Applications*. Springer-Verlag, Germany, 2001.
- [2] G.S. Duesberg, A.P. Graham, F. Kreupl, M. Liebau, R. Seidel, E. Unger, and W. Hoenlein. Ways towards the scaleable integration of carbon nanotubes into silicon based technology. *Diamond and related Materials*, 13:354, 2006.
- [3] N. Hamada, S. Sawada, and A. Oshiyama. New one-dimensional conductors: Graphitic microtubules. *Physical Review Letters*, 68:1579, 1992.
- [4] S. Iijima. Helical microtubules of graphitic carbon. *Nature*, 56:354, 1991.
- [5] A. Krishnan, E. Dujardin, T.W. Ebessen, P.N. Yianilos, and M.M.J. Treacy. Young modulus of single-walled nanotubes. *Physical Review B*, 58:14013, 1998.
- [6] J.P. Salvetat, G.A.D. Briggs, J.M. Bonard, R. Bacsá, A.J. Kulik, T. Stckli, N. Burnham, and L. Forró. Elastic and shear moduli of single-walled carbon nanotube ropes. *Physical Review Letters*, 82:944, 1999.
- [7] HJ Choi, J Ihm, SG Louie, and ML Cohen. Defects, quasibound states, and quantum conductance in metallic carbon nanotubes. *Physical Review Letters*, 84:2917–2920, MAR 27 2000.
- [8] P. Ayala, M. H. Ruemmeli, T. Gemming, E. Kauppinen, H. Kuzmany, and T. Pichler. Cvd growth of single-walled b-doped carbon nanotubes. *Physica Status Solidi B*, 245:1935–1938, OCT 2008.
- [9] Jae-Yel Yi and J. Bernholc. Atomic structure and doping of microtubules. *Physical Review B*, 47:1708–1711, Jan 1993.
- [10] R. Saito, G. Dresselhaus, and M.S. Dresselhaus. *Physical Properties of Carbon Nanotubes*. Imperial College Press, London, 1998.

- [11] M. S. Dresselhaus, G. Dresselhaus, R. Saito, and A. Jorio. Raman spectroscopy of carbon nanotubes. *Physics Reports-Review Section of Physics Letters*, 409:47–99, 2005.
- [12] S. Reich, C. Thomsen, and J. Maultzsch. *Carbon Nanotubes: basic concepts and physical properties*. Wiley-VCH, 2004.
- [13] H. Kataura, Y. Kumazawa, Y. Maniwa, I. Umezu, S. Suzuki, Y. Ohtsuka, and Y. Achiba. Optical properties of single-wall carbon nanotubes. *Synthetic Metals*, 103:2555, 1999.
- [14] PM Ajayan and S Iijima. Capillarity-induced filling of carbon nanotubes. *Nature*, 361(6410):333–334, JAN 28 1993.
- [15] Paola Ayala, Raul Arenal, Annick Loiseau, Angel Rubio, and Thomas Pichler. The physical and chemical properties of heteronanotubes. *Rev. Mod. Phys.*, 82(2):1843–1885, Jun 2010.
- [16] W. Cermigniani, T.E. Paulson, C. Onneby, and C.G. Pantalo. Synthesis and characterization of boron-doped carbons. *Carbon*, 33:367, 1995.
- [17] J.V. Zanchetta and A. Marchand. Electronic properties of nitrogen doped carbons. *Carbon*, 3:332, 1965.
- [18] DL Carroll, P Redlich, PM Ajayan, S Curran, S Roth, and M Ruhle. Spatial variations in the electronic structure of pure and b-doped nanotubes. *Carbon*, 36:753, 1998.
- [19] A. Quandt, C. Özdogbreve, J. Kunstmann, and Fehske H. Boron doped graphene nanostructures. *Physica Status Solidi B*, 245:2077–2081, 2008.
- [20] L Wirtz and A Rubio. Band structure of boron doped carbon nanotubes. *Molecular Nanostructures*, 685:402, 2003.
- [21] GG Fuentes, E Borowiak-Palen, M Knupfer, T Pichler, J Fink, L Wirtz, and A Rubio. Formation and electronic properties of bc₃single-wall nanotubes upon boron substitution of carbon nanotubes. *Physical Review B*, 69:245403, JUN 2004.
- [22] R Tenne and AK Zetl. Nanotubes from inorganic materials. In *Carbon Nanotubes*, volume 80, pages 81–112. 2001.
- [23] M Terrones, N Grobert, and H Terrones. Synthetic routes to nanoscale bxcynz architectures. *Carbon*, 40:1665–1684, 2002.

- [24] O Stephan and PM Ajayan. Doping graphitic and carbon nanotube structures with boron and nitrogen. *Science*, 266:1863–1685, 1994.
- [25] Jun Ma, Shuguang Guan, and C. H. Lai. Disorder effect on electronic and optical properties of doped carbon nanotubes. *Physical Review B*, 74:205401, NOV 2006.
- [26] R. Arenal, M. Kociak, and N. J. Zaluzec. High-angular-resolution electron energy loss spectroscopy of hexagonal boron nitride. *Applied Physics Letters*, 90:204105, 2007.
- [27] M. H. Ruemmel, C. Kramberger, M. Loeffler, M. Kalbac, H.-W. Huebers, A. Grueneis, A. Barreiro, D. Grimm, P. Ayala, T. Gemming, F. Schaeffel, L. Dunsch, B. Buechner, and T. Pichler. Synthesis of single wall carbon nanotubes with invariant diameters using a modified laser assisted chemical vapour deposition route. *Nanotechnology*, 17:5469–5473, NOV 14 2006.
- [28] F. Xu, M. Minniti, P. Barone, A. Sindona, A. Bonanno, and A. Oliva. Nitrogen doping of single walled carbon nanotubes by low energy ion implantation. *Carbon*, 46:1489 – 1496, 2008.
- [29] Shifeng Xu, Yi Fan, Jingsong Luo, Ligong Zhang, Wenquan Wang, Bin Yao, and Linan An. Phonon characteristics and photoluminescence of bamboo structured silicon-doped boron nitride multiwall nanotubes. *Applied Physics Letters*, 90:013115, JAN 1 2007.
- [30] F. Xu, M. Minniti, P. Barone, A. Sindona, A. Bonano, and A. Oliva. Nitrogen doping in single walled carbon nanotubes by low energy n²⁺ implantation. *Carbon*, 46:1489, 2008.
- [31] F. Villalpando-Paez, A. Zamudio, A. L. Elias, H. Son, E. B. Barros, S. G. Chou, Y. A. Kim, H. Muramatsu, T. Hayashi, J. Kong, H. Terrones, G. Dresselhaus, M. Endo, M. Terrones, and M.S. Dresselhaus. Synthesis and characterization of long strands of nitrogen-doped single-walled carbon nanotubes. *Chemical Physics Letters*, 424:345–352, 2006.
- [32] M. H. Rummeli A. Gruneis P. Ayala, F. L. Freire and T.Pichler. *J. Chem. Phys.*, 127, 2007.
- [33] Yo-Sep Min, Eun Ju Bae, Igor P. Asanov, Un Jeong Kim, and Wanjun Park. Growth and characterization of nitrogen-doped single-walled carbon nanotubes by water-plasma chemical vapour deposition. *Nanotechnology*, 18:285601, JUL 18 2007.

- [34] J. Luo, J. Hudson, J. Chen, G. Keskar, R. Rao and A. M. Rao. *Chem. Phys. Lett.*, 412, 2005.
- [35] E.I. Kauppinen, A. Moisala, A.G. Nasibulin, S.D. Shandakov, and Hua Jiang. On-line detection of single-walled carbon nanotube formation during aerosol synthesis methods. *Carbon*, 43(10):2066–74, August 2005.
- [36] Albert G. Nasibulin, Peter V. Pikhitsa, Hua Jiang, and Esko I. Kauppinen. Correlation between catalyst particle and single-walled carbon nanotube diameters. *Carbon*, 43(11):2251 – 2257, 2005.
- [37] Albert G. Nasibulin, Anna Moisala, David P. Brown, Hua Jiang, and Esko I. Kauppinen. A novel aerosol method for single walled carbon nanotube synthesis. *Chemical Physics Letters*, 402(1-3):227 – 232, 2005.
- [38] Albert G. Nasibulin, David P. Brown, Paula Queipo, David Gonzalez, Hua Jiang, and Esko I. Kauppinen. An essential role of CO_2 and H_2O during single-walled CNT synthesis from carbon monoxide. *Chemical Physics Letters*, 417(1-3):179 – 184, 2006.
- [39] P. Ayala, W. Plank, A. Grneis, E.I. Kauppinen, M.H. Rümmele, H. Kuzmany, and T. Pichler. A one step approach to b-doped single-walled carbon nanotubes. *Journal of Materials Chemistry*, 18:5676, 2008.
- [40] P. Ayala, A. Grueneis, D. Grimm, C. Kramberger, R. Engelhard, M. Rümmele, J. Schumann, R. Kaltofen, B. Buechner, C. Schaman, H. Kuzmany, T. Gemming, A. Barreiro, and T. Pichler. Cyclohexane triggers staged growth of pure and vertically aligned single wall carbon nanotubes. *Chemical Physics Letters*, 454:332–336, MAR 20 2008.
- [41] D. Grimm, A. Grüneis, C. Kramberger, M.H. Rümmele, A. Barreiro, T. Pichler, H. Kuzmany, and B. Büchner. Optimizing the chemical vapor deposition synthesis of single wall carbon nanotubes using n-heptane as carbon source. *Chemical Physics Letters*, 428:416, 2006.
- [42] B. Kitiyanan, W. E. Alvarez, J. H. Harwell, and D. E. Resasco. Controlled production of single-wall carbon nanotubes by catalytic decomposition of CO on bimetallic Co-Mo catalysts. *Chemical Physics Letters*, 317:497 – 503, 2000.
- [43] A. Jorio, R. Saito, J. H. Hafner, C. M. Lieber, M. Hunter, T. McClure, G. Dresselhaus, and M. S. Dresselhaus. Structural (n, m) determination of isolated single-wall carbon nanotubes by resonant Raman scattering. *Physical Review Letters*, 86:1118–1121, 2001.

- [44] F. Wang L. Huang X. M. H. Huang M. Huang J. Hone S. O'Brien J. A. Misewich T. F. Heinz L. Wu Y. Zhu L. E. Brus M. Y. Sfeir, T. Beetz. Optical spectroscopy of individual single-walled carbon nanotubes of defined chiral structure. *Science*, 312, 2006.
- [45] P. Finnie Y. Homma J. Lefebvre, J. M. Fraser. Photoluminescence from an individual single-walled carbon nanotube. *Phys. Rev. B*, 69, 2004.
- [46] T. Hertel R. B. Weisman G. Dresselhaus M. S. Dresselhaus A. Jorio, R. Saito. Carbon nanotube photophysics. *MRS Bull.*, 29, 2004.
- [47] A. Jorio, M.S. Dresselhaus, and G. Dresselhaus. *Carbon Nanotubes: Advanced Topics in the Synthesis, Structure, Properties and Applications*. Springer-Verlag, Heidelberg, 2008.
- [48] G. Dresselhaus A. Jorio, R. Saito and M.S. Dresselhaus. *Phil. Trans. R. Soc. Lond.A.*, 362, 2004.
- [49] O. Dubay and G. Kresse. Density functional calculations for c60 peapods. *Phys. Rev. B*, 70(16):165424, Oct 2004.
- [50] Cristiano Fantini Riichiro Saito and Jie Jiang. *Excitonic States and Resonance Raman Spectroscopy of Single-Wall Carbon Nanotubes*, chapter 8. Springer, 2008.
- [51] S. Empedocles M. Bawendi E. B. Hanlon A. M. Rao P. C. Eklund R. E. Smalley G. Dresselhaus M. S. Dresselhaus M. A. Pimenta, A. Marucci. Raman modes of metallic carbon nanotubes. *Phys. Rev. B Rapid*, 58, 1998.
- [52] F. Mauri A. C. Ferrari J. Robertson M. Lazzeri, S. Piscanec. Phonon linewidths and electronphonon coupling in graphite and nanotubes. *Phys. Rev. B*, 73, 2006.
- [53] A. G. Souza Filho G. Dresselhaus M. S. Dresselhaus M. A. Pimenta R. Saito, A. Jorio. Probing phonon dispersion relations of graphite by double resonance raman scattering,. *Phys. Rev. Lett.*, 88, 2002.
- [54] S. Reich C. Thomsen. Symmetry of the high-energy modes in carbon nanotubes. *Phys. Rev. Lett.*, 85, 2000.
- [55] G. G. Samsonidze V. Brar G. Dresselhaus M. S. Dresselhaus A. Jorio L. G. Cancado C. Fantini M. A. Pimenta A. G. Souza Filho R. Saito, A. Gruneis. Double resonance raman spectroscopy of single wall carbon nanotubes. *New J. Phys.*, 5, 2003.

- [56] S. D. M. Brown A. G. Souza Filho G. Dresselhaus J. H. Hafner C. M. Lieber R. Saito M. S. Dresselhaus M. A. Pimenta, A. Jorio. Diameter dependence of the raman d-band in isolated single-wall carbon nanotubes. *Phys. Rev. B*, 64, 2001.
- [57] I.O. Maciel, N. Anderson, M.A. Pimenta, A. Hartschuh, H. Quian, M. Terrones, H. Terrones, J. Campos-Delgado, A.M. Rao, L. Novotny, and A. Jorio. Electron and phonon renormalization near charged defects in carbon nanotubes. *Nature Materials*, 7:878–883, 2008.
- [58] A. Jorio A. G. Souza Filho A. Gruneis M. A. Pimenta G. Dresselhaus M. S. Dresselhaus G. G. Samsonidze, R. Saito. Phonon trigonal warping effect in graphite and carbon nanotubes. *Phys. Rev. Lett.*, 90, 2003.
- [59] Large-scale purification of single-wall carbon nanotubes: process, product, and characterization. *Applied Physics A: Materials Science & Processing*, 67:29–37, 1998.
- [60] Gene Dresselhaus (Editor) Mildred S. Dresselhaus (Editor) Ado Jorio (Author, Editor), editor. *Carbon Nanotubes: Advanced Topics in the Synthesis, Structure, Properties and Applications (Topics in Applied Physics)*. Springer, 2008.
- [61] C. Kittrell R. H. Hauge R. E. Smalley R. B. Weisman S. M. Bachilo, M. S. Strano. Structure-assigned optical spectra of single-walled carbon nanotubes. *Science*, 298, 2002.
- [62] J. Jiang, R. Saito, K. Sato, J. S. Park, Ge. G. Samsonidze, A. Jorio, G. Dresselhaus, and M. S. Dresselhaus. Exciton-photon, exciton-phonon matrix elements, and resonant raman intensity of single-wall carbon nanotubes. *Phys. Rev. B*, 75(3):035405, Jan 2007.
- [63] R. Arenal, F. de la Pena, O. Stephan, M. Walls, M. Tence, A. Loiseau, and C. Colliex. Extending the analysis of eels spectrum-imaging data, from elemental to bond mapping in complex nanostructures. *Ultramicroscopy*, 109:32–38, 2008.
- [64] M Glerup, J Steinmetz, D Samaille, O Stephan, S Enouz, A Loiseau, S Roth, and P Bernier. Synthesis of n-doped swnt using the arc-discharge procedure. *Chemical Physics Letters*, 387:193–197, MAR 21 2004.
- [65] H. Lin, R. Arenal, S. Enouz-Vedrenne, O. Stephan, and A. Loiseau. Nitrogen configuration in individual cnx-swnts synthesized by laser vaporization technique. *Journal of Physical Chemistry C*, 113:9509–9511, 2009.

- [66] P. Ayala, A. Grüneis, T. Gemming, B. Büchner, M.H. Rummeli, D. Grimm, J. Schumann, R. Kaltofen, F.L. Freire Jr., and T. Pichler". Influence of the catalyst hydrogen pre-treatment on the growth of vertically aligned nitrogen-doped carbon nanotubes. *Chemistry of Materials*, 19:6131–6137, 2007.

Curriculum Vitae

- Date of Birth: November 29, 1985
- Birthplace: Tucumán, Argentina

Education

- Bachiller polimodal en Ciencias Naturales. Normal "Juan Bautista Alberdi" High School. Tucumán, Argentina. 2003.
- Bachelor in Physics (Bachiller Universitario en Física). University of Tucumán. Tucumán, Argentina. 2008.

Scientific Work

- **Ruiz Soria, Georgina**; Grinblat, F.; Vega, N.; Villafuerte, M.; Heluani, S.; Braunstein, G. *Electric Conduction Mechanisms of Thin Films of ZnO Doped with Sulfur*. Seoul, South Korea: EE.UU.. 2008. 3rd IUPAP International Conference on Women In Physics 2008.IUPAP, Working Group on Women in Physics.
- Toma Susi, Zhen Zhu, **Georgina Ruiz-Soria**, Raul Arenal, Paola Ayala, Albert G. Nasibulin, Hong Lin, Hua Jiang, Odile Stephan, Thomas Pichler, Annick Loiseau and Esko I. Kauppinen. *Armchair-enriched nitrogen-doped SWCNTs synthesized in the presence of ammonia*.2010.(In press).

Poster

- **Ruiz Soria, Georgina**; Grinblat, F.; Vega, N.; Villafuerte, M.; Heluani, S.; Braunstein, G. *Electric Conduction Mechanisms of Thin Films of ZnO Doped with Sulfur*. 1st Conference AFA-SUF. Buenos Aires, Argentina. 2008.